ADVANCED HEALTHCARE MATERIALS
www.advhealthmat.de

Cell-Derived Vesicles for Nanoparticles' Coating: Biomimetic Approaches for Enhanced Blood Circulation and Cancer Therapy

Carolina F. Rodrigues, Natanael Fernandes, Duarte de Melo-Diogo, Ilídio J. Correia, and André F. Moreira**

Cancer nanomedicines are designed to encapsulate different therapeutic agents, prevent their premature release, and deliver them specifically to cancer cells, due to their ability to preferentially accumulate in tumor tissue. However, after intravenous administration, nanoparticles immediately interact with biological components that facilitate their recognition by the immune system, being rapidly removed from circulation. Reports show that less than 1% of the administered nanoparticles effectively reach the tumor site. This suboptimal pharmacokinetic profile is pointed out as one of the main factors for the nanoparticles' suboptimal therapeutic effectiveness and poor translation to the clinic. Therefore, an extended blood circulation time may be crucial to increase the nanoparticles' chances of being accumulated in the tumor and promote a site-specific delivery of therapeutic agents. For that purpose, the understanding of the forces that govern the nanoparticles' interaction with biological components and the impact of the physicochemical properties on the in vivo fate will allow the development of novel and more effective nanomedicines. Therefore, in this review, the nano–bio interactions are summarized. Moreover, the application of cell-derived vesicles for extending the blood circulation time and tumor accumulation is reviewed, focusing on the advantages and shortcomings of each cell source.

1. Introduction

Nanoparticles' application in medicine created a new era of cancer research, from diagnostic to therapeutic.[1,2] Particularly, nanomaterials have been showing the potential for overcoming the pharmacokinetic limitations and reducing the side effects of conventional cancer therapies. Until now, several nanomedicines have already been approved for cancer treatment, such as Doxil, Abraxane, Vyxeos, and many others are currently under clinical trials.[3,4] These nanomedicines demonstrate numerous advantages over the administration of free chemotherapeutic drugs: prolonged circulation time, improved drug solubility, enhanced bioavailability, and lower side effects.[5,6] Nonetheless, despite several studies demonstrating the potential of nanoparticles as selective drug delivery platforms and effectively induce cancer cells' death both in vitro and in vivo, the application of nanomedicines in the treatment of human tumors often presents modest improvements in the overall survival rate of patients. In fact, only 0.7% of the nanoparticles' injected dose effectively reaches the tumor site.[7] Thus, this still suboptimal nanoparticles' pharmacokinetics is pointed out as one of the main factors for its reduced therapeutic effectiveness and its poor translation into clinical practice. Such is further supported by the rather limited knowledge of the interactions between nanoparticles and living organisms, namely humans.[8–11]

Nevertheless, there is a consensus that longer circulation times are crucial to increasing the chances of nanoparticles being accumulated in the tumor microenvironment.[12,13] Classically, researchers have been focusing on passive or active targeting strategies to improve the specific delivery of the therapeutics to cancer cells, exploring mainly the enhanced permeability and retention (EPR) effect or the so-called vascular bursts.[14,15] However, once in the body, nanoparticles can immediately interact with biological components (e.g., proteins and cells). Particularly, the interactions between nanoparticles and physiological fluids are induced by several forces that will determine the formation of a protein corona. The protein corona can induce several modifications in the nanomedicines' initial properties

C. F. Rodrigues, N. Fernandes, D. de Melo-Diogo, I. J. Correia, A. F. Moreira
CICS-UBI – Health Sciences Research Centre
Universidade da Beira Interior
Av. Infante D. Henrique, Covilhã 6200-506, Portugal
E-mail: icorreia@fcsaude.ubi.pt; afmoreira@fcsaude.ubi.pt

A. F. Moreira
CPIRN-UDI/IPG – Center of Potential and Innovation in Natural Resources, Research Unit for Inland Development
Instituto Politécnico da Guarda
Avenida Dr. Francisco de Sá Carneiro, Guarda 6300-559, Portugal

The ORCID identification number(s) for the author(s) of this article can be found under https://doi.org/10.1002/adhm.202201214

DOI: 10.1002/adhm.202201214

(e.g., hydrodynamic size, surface chemistry, hydrophobicity, immunogenicity) that will impact nanoparticles' blood retention, bioavailability, tumor accumulation, and even their biosafety.[16,17] Thus, the nanoparticles' surface properties play a huge role in the nanoparticles' behavior. Understanding the interactions that can be established between nanoparticles and biologic systems, as well as the modulation of nanoparticles' surface physicochemical properties will allow us to predict the forces that govern the nano–bio interactions, and consequently the nanomedicines' biological fate and efficacy in cancer therapy.[9,12] In recent years, different strategies have been developed to improve nanoparticles' circulation time, mainly by the optimization of their physicochemical properties and functionalization with hydrophilic polymers or biomimetic coatings.[18–20] Particularly, the creation of biomimetic coatings based on cell-derived vesicles is an emerging concept to improve the nanomaterials' biological performance. These cell-derived vesicles inherit the unique features of the source cells, such as biocompatibility, long circulation time, homologous targeting, and immune evasion, showing a high potential to create novel and more effective cancer therapies.[21,22] Therefore, in this review, an overview of the practical approaches described in the literature to prolong nanoparticles' blood circulation is provided. Initially, the nanoparticles' application in cancer therapy and their biological and physicochemical interactions in the bloodstream will be discussed. Then, the different strategies exploring the application of biomimetic coatings based on the utilization of cell-derived vesicles are also overviewed, highlighting their potential for increasing the nanomaterials' blood circulation and tumor accumulation.

2. Nanomaterials in Cancer Therapy

The administration of nanomedicines in the human body, particularly in cancer therapy, is generally performed through the intravenous route.[23] From the administration until reaching the cancer cells and the subsequent delivery of the therapeutic agents, nanoparticles undergo a process that comprises five major steps (CAPIR cascade): blood **C**irculation, tumor **A**ccumulation, **P**enetration into the tumor tissue, cellular **I**nternalization, and drug **R**elease.[24] In fact, the overall therapeutic efficacy of drug delivery systems largely depends on the effectiveness of each one of these steps. Once in the bloodstream, nanoparticles should be stable (i.e., sidestep degradation, oxidation, aggregation) and also avoid interaction with proteins. Upon intravenous administration, the nanoparticles are susceptible to the adsorption of plasma proteins (e.g., serum albumin, immunoglobulins, and complement compounds) on their surface, which can induce nanoparticles' physiochemical changes (e.g., aggregation and increase of the hydrodynamic size).[17,25] These modifications can facilitate the nanoparticles' recognition by phagocytic cells, blood clearance, and/or the accumulation in off-target tissues, such as the reticuloendothelial system (RES) organs (e.g., spleen and liver), which consequently results in shortened blood circulation times (**Figure 1**).[25]

When in circulation, nanoparticles must be able to reach and accumulate passively in the tumor tissue, making use of the EPR effect.[14,26] This phenomenon arises from the leaky and abnormal tumor vasculature (i.e., capillaries with fenestraes' sizes between 200 and 1200 nm) and the impaired lymphatic drainage resulting from the fast and uncontrolled cellular proliferation in the tumor, which enable the extravasation of nanoparticles from the bloodstream followed by its retention in the tumor tissue.[27] Besides the EPR effect, the occurrence of transient and dynamic vascular bursts/eruptions in tumor vessels was recently described as an alternative event that mediates the diffusion of nanomedicines from blood to the tumor interstitial space.[15] Therefore, nanoparticles' size, shape, and blood circulation time are crucial factors that will mediate the nanoparticles' capacity to take advantage of the EPR and/or dynamic vascular bursts/eruptions.[26,28] However, it is worth noticing that this passive accumulation phenomenon is more pronounced in animal tumors, whereas in human tumors the EPR can be absent.[28,29] The type of tumor, the size, the location, the development stage, the blood flow, and the structural complexity are some factors that influence the intensity of the EPR effect.[29,30] Therefore, to further increase the nanoparticles' specificity to the tumor tissue, researchers have also been exploring active targeting strategies. These strategies focus on the functionalization of nanoparticles with targeting moieties that specifically recognize the molecules overexpressed at the tumor site or in newly formed vessels, favoring the nanoparticles' interaction and accumulation in these areas.[31,32] After nanoparticles reach and accumulate in the tumor tissue, the process can become more complex. The penetration and diffusion of nanoparticles in a solid tumor are hindered by the heterogeneous distribution of blood vessels, the high interstitial pressure, the tumor's dense extracellular matrix, and the highly compacted cancer cells. Altogether, the ability of a high dose of nanoparticles to diffuse and reach the center of the tumor is compromised, leading to a heterogeneous, superficial, and reduced distribution of the nanoparticles.[33,34]

Finally, the cell membrane is the last natural barrier that nanoparticles have to surpass to release their cargo into the intracellular space and exert their therapeutic effect. The nanocarriers are mainly internalized by endocytosis and the utilization of targeting molecules can confer to the nanoparticles a higher specificity toward cancer cells.[35] However, the cancer cells present mechanisms, such as the overexpression of P-glycoproteins, that can avoid the intracellular accumulation of anticancer drugs impairing the therapeutics' effectiveness.[36] However, the latest data analysis refers that ≈99% of the intravenously administered nanoparticles do not reach the tumor tissue.[7] Therefore, the enhancement of the nanoparticles' CAPIR cascade is an actual and prominent target for researchers. In this field, there are two major focuses i) increasing the nanoparticles' blood circulation time and ii) developing nanoparticles with higher specificity to cancer cells.[22,24] Considering the CAPIR cascade, the first step to increase the nanoparticles' accumulation in the tumor tissue should encompass the optimization of the nanoparticles' pharmacokinetics, starting with the blood circulation time. This consensus is related to the higher probability of the nanoparticles pass by the tumor site and interact with the tumor cells.[13,22,37] Moreover, the combination of higher blood circulation times with the introduction of active targeting moieties may further boost the therapeutic potential of the nanomaterials.[14,38] In the following sections, the nano–bio interactions will be described as well as the different strategies exploring the application of cell-derived vesicles for increasing the nanomaterials' blood circulation and tumor accumulation.

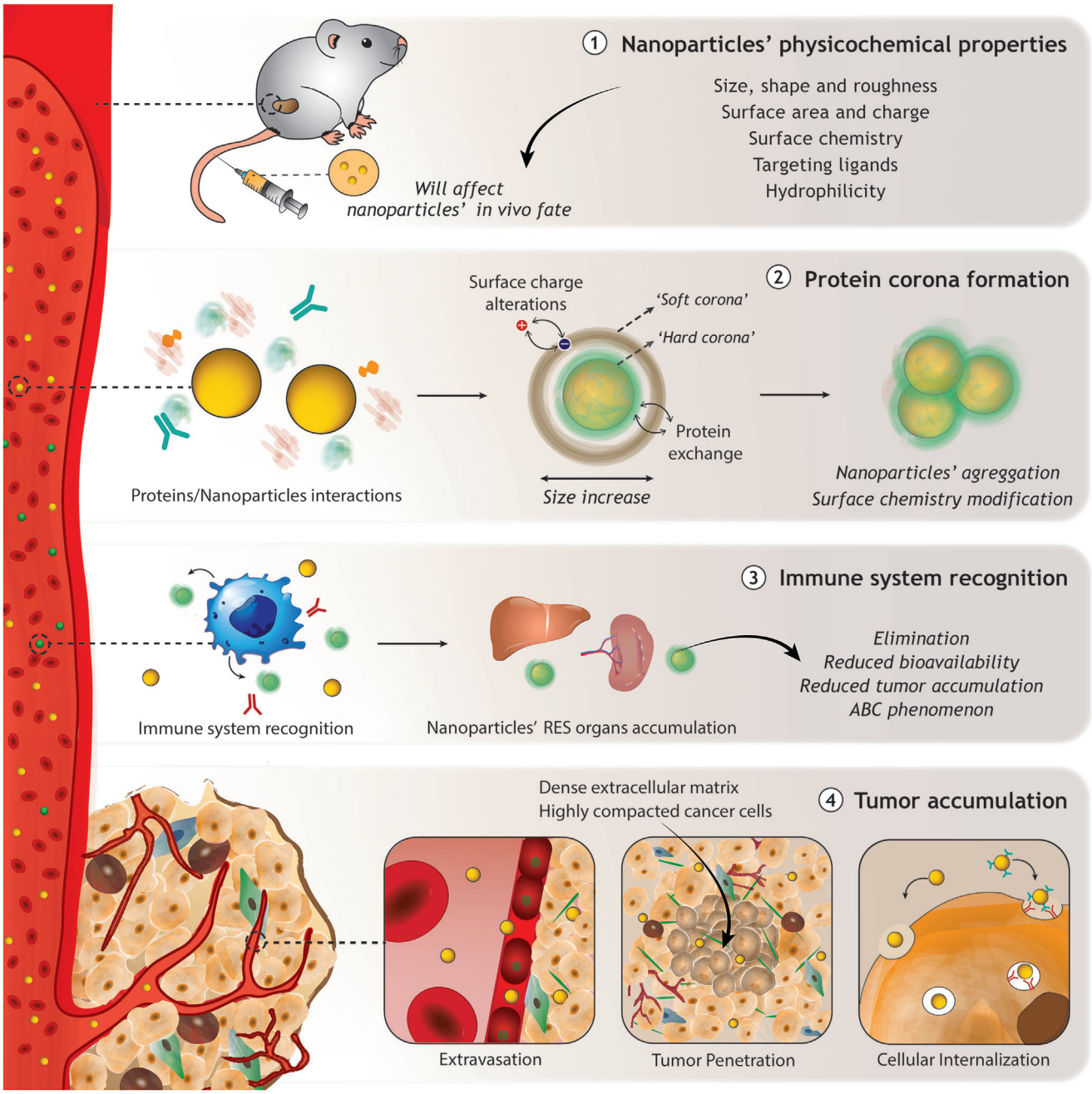

Figure 1. Representation of the main factors and processes that nanoparticles undergo from their administration until their accumulation in the tumor. 1) Nanomaterials' physicochemical properties impact all the processes along the CAPIR cascade, particularly the blood circulation time, and consequently nanomaterials in vivo fate. 2) Once in the bloodstream nanoparticles can interact with blood proteins, resulting in the formation of a protein corona that will induce several changes in nanomaterials' properties, which can lead to 3) the activation of the immune system and premature elimination of nanomaterials. 4) The nanomaterials that can effectively reach the tumor, need to surpass the tumor vasculature, penetrate the highly compacted tumor region, and to be internalized by cancer cells to exert their therapeutic effect.

3. Nano–Bio Interactions in Blood Circulation

3.1. Protein Corona

Once in the body, nanoparticles interact with the biological compounds establishing a nano–bio interface, that is constituted by the nanoparticle's surface; the solid–liquid interface (formed when the particle interacts with the biological fluids), and the contact zone of this solid–liquid interface with the biological system.[25] Biological fluids (e.g., blood and interstitial fluid) present a high protein content. Since most nanomedicines are intravenously administered, the absorption of blood proteins is the most discussed in the literature. Blood is a highly complex fluid composed of cellular and acellular elements. The protein

fraction of the blood represents ≈4% of the total volume and is composed of albumin, globulin, complement components, coagulation factors, and apolipoproteins.[39] Upon administration, nanoparticles can be rapidly covered by a high abundance of proteins, which are adsorbed with low affinity, forming a dynamic protein corona (called "soft corona," Figure 1). After a few minutes, the soft corona is replaced by proteins with higher affinity, which are strongly adsorbed to nanoparticles' surface—called "hard corona".[17,25,40,41] Therefore, the nano–proteins interaction is also denominated as the first nano–bio interface of nanomedicines.[25] The protein corona will induce several changes in the nanomaterial physicochemical properties (e.g., aggregation state, hydrodynamic size, surface charge, and surface chemistry), which can be very distinct from its synthetic identity and compromise its therapeutic performance. Moreover, the adsorbed proteins may induce RES activation and accelerate the nanoparticles' elimination. Additionally, the adsorbed proteins can also participate in the activation of a series of signaling cascades that can lead to coagulation and/or anaphylactic shock.[25,41,42]

3.2. Nano–Bio Interactions and Nanoparticles' Physiochemical Properties

Nanoparticles' surface properties (e.g., size, shape, surface area, roughness, porosity, hydrophilicity, and chemical composition) will determine their interaction with the biological fluids and the composition of the protein corona. However, some properties such as surface charge, stability, biodegradability, or aggregation state can also be determined by the biological fluids (e.g., pH and ionic force).[25] The nanoparticles' surface properties are decisive in the affinity and degree of proteins to be adsorbed and also determine the forces that govern the nano–protein interface, such as hydrogen bonding, van der Waals (VDW), electrostatic, and hydrophobic interactions.[25] Nanomaterials with charged groups on their surface (e.g., carboxylic acid or amines) can trigger electrostatic interactions with ionized proteins. Although different ions are present in the bloodstream, normally the interaction of nanomaterials with macromolecules is comparatively more favorable and stable. VDW forces also occur, however they correspond to short-range and weak electrostatic attractions that are dependent on the positioning of the atoms at the nanoparticles' surface.[25,40,43,44] Additionally, hydrogen bonding can occur between polar residues on the nanoparticles' surface (e.g., hydroxyl groups) and hydrophilic uncharged regions present in proteins (e.g., serine, glutamine residues). Although these interactions are stronger than VDW forces, their frequency of occurrence is low in biological fluids. Moreover, hydrophobic interactions may also occur on the surface of certain materials (e.g., polystyrene). In addition to the chemical composition of the nanoparticle's surface, other physicochemical properties can affect protein adsorption. For example, smaller nanoparticles with greater curvature tend to promote higher protein adsorption (due to reduced interactions between proteins). Proteins with an isoelectric point >5.5 have more affinity for positively charged nanoparticles, whereas proteins with an isoelectric point <5.5 have more affinity for negatively charged nanosystems. In addition, roughness and hydrophobicity can also affect the nano–protein interaction. The highly hydrophobic nanoparticles tend to stabilize the adsorption of proteins on their surface (i.e., will potentiate the action of opsonins), while a rougher surface often leads to increased adsorption of proteins as well as interaction with cells.[25,40,41,45,46]

Altogether, these nano–protein interactions could largely change nanoparticles' surface and dictate their blood circulation time and bioavailability.[41,46] For example, nanoparticles with sizes inferior to 5 nm can be rapidly eliminated by renal filtration, whereas sizes lower than 50 nm can accumulate in hepatocytes. Nanoparticles larger than 200 nm accumulate in the spleen and can also be sequestered by macrophages present in the RES main organs. Considering these values and those imposed by the EPR effect, the desirable nanoparticle size for intravenous administration should be in the range between 100 and 200 nm.[26,47] As described above, charged nanoparticles tend to interact with plasma proteins, being a neutral charge (±10 mV) considered ideal for minimizing opsonization or RES uptake.[48,8] Furthermore, nanoparticles' shape (e.g., spheres, rods, sheets) can also influence the nanoparticles' circulation time and play an important role in their in vivo fate.[12,49] The shape determines the nanoparticle's location in the blood vessels (central or peripherical zone). Spherical nanomedicines tend to circulate in the center of the vessels, whereas anisotropic nanostructures tend to circulate closer to the walls of the blood vessels. In this case, the nanoparticles' interaction with the tumor vasculature is beneficial and will improve the probability of nanoparticles accumulating in this tissue.[50] Additionally, in the bloodstream, the nanoparticles' shape can mediate the interaction and recognition by RES. Black et al. observed a lower RES uptake and consequently, a higher blood circulation for gold nanospheres when compared with gold nanorods and nanocages.[51] However, this topic is also a subject of strong debate, with other studies revealing that anisotropic-shaped nanoparticles present a lower macrophage interaction and higher circulation time, when compared with spherical counterparts.[52] Thus, the nanomedicines' design, considering the optimal physicochemical characteristics, is fundamental to reduce the formation of a protein corona and, consequently, prolong the blood circulation time.

3.3. Surface Functionalization to Modulate the Nano–Bio Interactions

Currently, the major strategies to prolong blood circulation are based on surface modifications with highly hydrophilic polymers or biomimetic materials.[22,53] These surface modifications minimize the proteins' adsorption, reducing the changes in the nanomaterials' size and charge as well as the recognition and elimination by the immune system. The selection of polymers for drug delivery systems must fulfill the general properties for biological applications, namely non-immunogenicity, biocompatibility, stability, and biodegradability (or easy excretion after the desirable therapy).[54] Polymers with antifouling properties are desirable since they can resist nonspecific protein adsorption and cell adhesion, which significantly attenuate the immune system recognition, improving the pharmacokinetic profile.[53,55] These antifouling properties can be explained by two main theories. The so-called "steric repulsion" considers that the compression of the polymeric chains as the proteins approach the polymeric surfaces

avoids the formation of the protein corona. In this process, the surface density of the grafted polymers plays a critical role in the resistance to protein adsorption. Otherwise, the second theory—"water barrier"—describes that the hydration layer formed between the polymeric surfaces and the surrounded medium provides a repulsion force that can prevent protein adsorption.[56–58] Polyethylene glycol (PEG) is the most widely applied polymer in drug delivery due to its safety and stealth properties, being approved by Food and Drug Administration for use in drug delivery, pharmaceuticals, and cosmetics. Moreover, several PEGylated pharmaceuticals are under clinical trials and many others are already commercialized.[59] PEG is a neutral and highly hydrophilic polymer, that can create a dynamic and thick hydration shell that hinders the macromolecules' adsorption and cells' interaction with the PEGylated surface. In general, PEGylation has been shown to improve the stability, circulation lifetime, and consequently the therapeutic effect of several nanosystems (e.g., micelles, liposomes, and gold nanoparticles, among others).[59–62] Once in solution, each ethylene glycol subunit is surrounded by at least 2–3 water molecules which render a large hydration shell that sterically prevents the interaction and penetration of biological compounds into the polymer layer. The water molecules near PEG terminal groups are also crucial for limiting protein adsorption, where a large number of tightly bound water molecules around the terminal groups of PEG induce a strong repulsive force.[63] Additionally, PEG presents high flexibility, mobility, and conformation that make the displacement of PEG chains by biointeractions thermodynamically unfavorable. Therefore, PEG acts as a shield improving the in vivo stability of nanoparticles, preventing the nanoparticles' aggregation and interaction with blood components, reducing the clearance rate, and consequently prolonging nanosystems' blood circulation time.[64] However, many parameters can influence the interactions and circulation time of PEGylated nanoparticles, such as PEG molecular weight (Mw), density at the nanoparticle surface, and chain architecture. Different studies revealed that increasing the PEG Mw leads to higher in vivo circulation times, mainly by reducing nanoparticles' aggregation and formation of the protein corona.[60,61,65–67] Despite these advantages, some drawbacks have been limiting the translation of the PEGylated nanomaterials to the clinic. Several studies demonstrated that multiple administrations can stimulate anti-PEG antibody responses and accelerate the opsonization and clearance of PEGylated nanosystems—a phenomenon denominated by **a**ccelerated **b**lood **c**learance (ABC).[68] In fact, animals and humans that receive repeated doses of PEGylated therapeutics often generate potent IgM antibody responses to PEG, which causes a rapid elimination (minutes to a few hours) of the subsequent doses of PEGylated systems.[69–73] Interestingly, there is also an increasing number of people allergic to PEGylated materials and presenting anti-PEG antibodies without being exposed to PEGylated therapeutics, which can be related to the increased widespread consumption of products containing PEG (e.g., food and cosmetics).[74]

Other classes of polymers, with properties similar to PEG, have also been investigated in the last years.[18] Among them, the hydrophilic polymers, poly(2-oxazoline)s (POx), and poly(zwitterion)s, have been pointed out as the most promising substitutes. POx have emerged as a promising polymer class with diverse potential applications due to their good biocompatibility, high stability, and structural versatility. Also, POx can be easily conjugated with drugs/peptides/proteins, which increase their interest in drug delivery applications.[19,75] Particularly, the hydrophilic poly(2-ethyl-2-oxazoline) and poly(2-methyl-2-oxazoline) polymers have been highly studied and are considered suitable candidates to substitute the well-established PEG.[76,77] When compared to PEG, POx present a simpler synthesis process and higher structural versatility.[78] Similar to that described for PEG, the POx Mw will influence its pharmacokinetic profile, with a higher Mw generally resulting in longer blood circulation times and reduced clearance rates.[75,78,79] Different studies also indicate that the balance between longer circulation times and lower retention in clearance organs can be fine-tuned by optimizing POx's Mw as well as the main and side-chain length.[80] Despite the still limited clinical dissemination of POx, in comparison to PEG, their application in drug delivery has grown enormously in the last decade. The hydrophilicity of POx conjugated with their reduced interactions with biomolecules and cells is decisive for their excellent antifouling/stealth properties.[75] However, different reports have also been describing the establishment of the ABC phenomenon and immune responses against several materials, including POx polymers.[81,82] Therefore, with successive administrations, the effective dose that can reach the tumor tissue is decreased. In this way, the use of stealth polymers is no longer advantageous compared to uncoated particles, having as an aggravating factor, the possible toxicity triggered in the RES organs. Phagocytosed nanoparticles can be retained in RES organs for long periods, which can trigger acute or chronic toxicity. With this in mind, several strategies started to be investigated (e.g., increasing the time intervals between doses, administration of blank nanoparticles to saturate phagocytic cells, and using higher doses of nanoformulations in each administration) to minimize host immune responses or side effects.[83–85]

Alternatively, zwitterionic materials such as poly (sulfobetaine), poly(carboxybetaine), and phosphorylcholine-based polymers (e.g., 2-methacryloyloxyethyl phosphorylcholine) are also able to improve nanoparticles' circulation time.[86–89] One of the interests of zwitterionic polymers over hydrophilic polymers is its stimuli-responsive capacity that offers a powerful strategy for delivering and releasing cargos at the desirable site and time.[90] Zwitterionic polymers confer high stability and hydration to nanoparticles' surfaces, which strongly reduce protein adsorption, compared with PEGylated nanoparticles.[86,87,90,91] This nonfouling capacity arises from the zwitterionic polymers' unique chemistry, overall electrostatic neutrality, opposite charge distribution, and high chain hydration and flexibility.[92] The water molecules also play a huge influence in the zwitterionic nanoparticles' stealth behavior, and its nonfouling ability can be directly related to the hydration layer formed after the contact of nanomaterials' surface with the body fluids.[93] This higher surface' hydration and stability can be explained by the forces that operated in the interaction of the nanoparticles' surface with the biological fluids. While PEG interacts with water through hydrogen bonding, zwitterionic materials present stronger electrostatic interactions with water.[63,91,94] For example, sulfobetaine presents a larger binding capacity to water molecules when compared to PEG, which generates a more stable and firmer hydration layer.[91] Therefore, zwitterionic nanoparticles

present an improved resistance to the formation of the protein corona, avoiding the ABC phenomenon and consequently prolonging the nanoparticles' circulation time.[93,95,96] Nevertheless, this capacity also renders to zwitterionic coatings a reduced interaction with cells, which can difficult the uptake by cancer cells.[95,97,98] Therefore, the obtainment of nanoparticles that simultaneously present a prolonged circulation time (e.g., with antifouling properties) and improved cancer cell internalization can be challenging. Thus, in the last decade, there has been a great focus on developing biomimetic strategies for cancer treatment. The utilization of bioinspired coatings, such as naturally occurring polymers (e.g., collagen, gelatine, albumin, hyaluronic acid, folic acid, dextran), has been widely explored due to their abundance in nature, biocompatibility, and biodegradability. Moreover, proteins and polysaccharides-based functionalization presents similarities with the extracellular matrix and a highly hydrophilic character which contributes to a lesser invasive and non-immunogenic profile as well as extending the blood circulation time.[99,100,101] However, the suboptimal efficacies that are still noted have been pressuring the development of novel bioinspired approaches.

In the following topic, the biomimetic strategies based on self-membranes that have been developed to increase the nanomaterials' blood circulation time will be presented (**Table 1**). Moreover, the role of these surface modifications in modeling the nano–bio interactions will be reviewed emphasizing the impact on the CAPIR cascade, i.e., the nanoparticles' tumor accumulation.

4. Cell-Derived Vesicles

4.1. Techniques for Extraction and Production of Cell-Derived Vesicles and Nanoparticles' Coating

Recent advances in cellular biology and nanotechnology have led to the development of nanoparticles coated with vesicles derived from cell membranes. The introduction of vesicles derived from the patient's cytoplasmatic membranes acts as a natural long-circulating nanomaterial, with the ability to avoid immune recognition and surpass biological barriers.[20,22] These biomimetic nanoparticles present a "core–shell structure": nanoparticle core (organic/inorganic core with different therapeutic functionalities) and a cellular-derived vesicle layer (vesicles created from cytoplasmatic membranes) that mimics the antigenic diversity of the source cell and provides immune escape, targeting ability, and cellular related-functions.[21]

The cell-derived vesicles can be engineered from different types of cells such as non-nucleated (erythrocytes and platelets), immune (e.g., leukocytes, macrophages), and cancer cells.[102–105] In turn, their application in the nanoparticles' coating can be resumed in three main steps: i) the production of the nanoparticle core, ii) isolation and extraction of the desired cell membrane, and iii) formation of the cell-derived vesicle entrapping the nanoparticle core(s).[21,102,106] After the selection and proliferation of the source cell, different procedures can be used to promote the disruption of the cell membrane, such as mechanical (e.g., ultrasounds) and physical (e.g., osmotic shock and freeze–thaw cycles) processes. Then, several centrifugation/washing steps must be performed to remove the intracellular content (i.e., cytoplasmatic organelles and nucleus).[102,107–109] It is worth noticing that both the cell disruption and purification methods are dependent on the cell source to be used. For example, the utilization of nucleated cells increases the complexity of the purification step, being necessary to use gradient centrifugation methods to separate the cell membranes from the remaining cell residues.[110–113] Moreover, in general, the isolation procedure should be carried out at 4 °C using protease inhibitors, to preserve the multicomponent structure (i.e., lipids, proteins, carbohydrates) and intrinsic functionalities of the original membrane.[105,112] Then, different techniques (e.g., coextrusion, sonication, extrusion/sonication, and microfluidic electroporation) can be used to fuse the vesicles and the nanomaterials.[114–116] Usually, before this step, it is performed a preliminary extrusion of the purified cell membrane fragments through polycarbonate porous membranes, with well-defined pores (e.g., 50, 100, 200, or 400 nm), generating empty cell-derived vesicles.[112,116,117] In fact, the extrusion of the purified cell membrane fragments and/or coextrusion with the nanoparticles' cores is one of the most explored techniques to create nonloaded or nanoparticle-containing cell membrane-derived vesicles.[114] This process is based on several cycles of extrusion of the cell membrane fragments/nanoparticles suspension through polycarbonate porous membranes (e.g., a pore size of 50, 100, 200, or 400 nm), which homogenizes the size of the cell-derived vesicles to values close to the membrane pore. During the successive passages, the mechanical forces promote the reorganization of the vesicles promoting a core–shell organization due to the combination with the nanoparticle cores.[116–119] The number of extrusion cycles, the pore size, and the applied pressure are some of the factors that affect the diameter and size distributions of extruded materials.[120]

The sonication-based approaches explore the utilization of ultrasounds (frequencies ranging from 20 to 50 kHz), in an ultrasonic bath or probe sonicator, to promote the disruption of the cell-derived vesicles, favoring the interaction with the nanoparticle cores.[121–124] However, the ultrasounds energy can also lead to the sample's heating and consequently induce the denaturation of the proteins that compose the cell-derived vesicles. Moreover, the cavitation phenomena can also promote the destruction of the nanoparticle cores.[124,125] Therefore, the ultrasounds' frequency, power, and duration are factors that should be considered, during the sonication process, to increase the yield and homogeneity of the core–shell nanoparticles.[124] To address these issues, the sonication technique is often combined with extrusion approaches. This combination reduces the loss of cell membrane fragments and nanoparticle cores (observed during the repeated extrusion cycles) as well as increases the sample's size homogeneity.[108,116,124,126,127] Recently, microfluidic electroporation has also been applied to produce cell-derived vesicles containing nanoparticle cores. This strategy is based on electric pulses that facilitate the penetration of the nanoparticles' core into the cell-derived vesicles when the components are flowing through the electroporation zone.[115,128] In this process, the size of the cell-derived vesicle is defined by the diameter of the microfluidic channel. Rao et al. developed erythrocyte-derived vesicles camouflaged Fe_3O_4 magnetic nanoparticles through a microfluidic device that consists of two channels (a Y-shaped merging channel and an S-shaped mixing channel), two inlets, one electroporation zone, and one outlet.[115] The cell-derived vesicles and nanoparticles are injected into this system through the

Table 1. Overview of the biodistribution and circulation time of cell-derived vesicles camouflage nanoparticles for application in cancer therapy (N.D. – nondisclosed, N.A. – not applicable, PDI – polydispersity index).

Cell source	Nanoparticle core	Size [nm]	Charge [mV]	Cargo	Vesicles production/coating methodology	Circulation time	Biodistribution	Refs.
RBC	Fe_3O_4	98.2 (PDI = 0.239)	−9.8 ± 1.2	N.A.	Isolation from mice Vesicles production: physical process → centrifugation → extrusion Coating: extrusion	After 8 and 24 h of administration, the Fe_3O_4@RBC nanoparticles exhibited a blood retention of 18.3% and 14.2% ID g^{-1}, respectively. After 24 h, PEGylated Fe_3O_4 presented a blood retention lower than 6% ID g^{-1}. After 24 h of the second administration, Fe_3O_4@RBC presented blood retentions similar to those of the first administration, whereas PEGylated Fe_3O_4 nanoparticles' blood retention decreased from 5.5% to 1.8% ID g^{-1}.	Fe_3O_4@RBC nanoparticles presented lower liver and spleen accumulation (49.2 ± 7.1 and 100.1 ± 16.3 μg g^{-1} tissue), than PEGylated Fe_3O_4 nanoparticles (117.4 ± 30.3 and 174.5 ± 43.7 μg g^{-1}).	[108]
	Fe_3O_4	≈100	≈−10	N.A.	Isolation from mice Vesicles production: physical process → centrifugation → sonication → extrusion Coating: microfluidic electroporation or extrusion	RBC-coated nanoformulations (extrusion made (RBC@MNs-C) or microfluidic electroporation made (RBC@MNs-E)) presented ≈3 times higher blood retention over 8 to 48 h, than bare nanoparticles. RBC@MNs-E formulations exhibited increased blood retention.	RBC@MNs-E nanoparticles presented the highest tumor accumulation and reduced RES accumulation, followed by RBC@MNs-C and bare nanoparticles.	[115]
	Albumin (IPH)	180 (PDI = 0.15)	−16	ICG (indocyanine green)/ perfluorocarbon (PFC)	Isolation from mice Vesicles production: physical process → centrifugation → extrusion Coating: sonication → extrusion	The elimination lifetime of IPH@RBC nanoparticles was 15.71 h, almost 14-fold higher than ICG encapsulated in albumin nanoparticles and bare IPH nanoparticles. The ICG-loaded albumin and IPH-loaded nanoparticles were cleared within 24 h from the liver, whereas IPH@RBC nanoparticles were still detected in blood after 48 h.	RBC-derived vesicles reduced the uptake by RAW264.7 macrophages by ≈50%, when compared with bare IPH nanoparticles. After 48 h of administration, IPH@RBC nanoparticles are mainly accumulated in the tumor and liver, being the tumoral accumulation higher than in the liver. Also, IPH@RBC nanoparticles have a 5.6-fold higher tumor accumulation than the bare IPH nanoparticles.	[127]

(*Continued*)

Table 1. (Continued).

Cell source	Nanoparticle core	Size [nm]	Charge [mV]	Cargo	Vesicles production/coating methodology	Circulation time	Biodistribution	Refs.
	N.A.	≈150 (PDI = 0.216)	28	ICG/10-hydroxycamptothecin (10-HCPT)	Isolation from Sprague–Dawley rats Vesicles production: physical process → centrifugation → extrusion Coating: sonication → extrusion	After 24 h of injection, ≈16.3% ID g^{-1} of RBCs@ICG-HCPT nanoparticles were detected in the blood, whereas in the same period only ≈2.0% and 7.5% ID g^{-1} of free ICG and ICG-HCPT nanoparticles were detected, respectively.	Reduced accumulation in the liver and spleen (≈20% and ≈19% ID g^{-1}, respectively) and increased accumulation in the tumor (≈8% ID g^{-1}), when compared with ICG-HCPT nanoparticles (with ≈27%, 24%, and 5% ID g^{-1}, on liver, spleen, and tumor, respectively).	[129]
	Chitosan–PLGA	256 ± 4	−5.7 ± 0.3	5-fluorouracil (5-FU)	Isolation from Wistar rats Vesicles production: physical process → centrifugation → extrusion Coating: extrusion	The plasma concentration at 0.25 h of 5-FU-loaded RBC-coated nanoparticles (24.04 ± 3.0 μg mL^{-1}) was significantly higher than free 5-FU (12.96 ± 2.7 μg mL^{-1}) and 5-FU–chitosan–PLGA nanoparticles (17.85 ± 3.6 μg mL^{-1}). The plasma concentration after 24 h of administration decreased to 0.011, 1.9, and 6.5 μg mL^{-1} for free 5-FU, 5-FU–chitosan–PLGA nanoparticles, and 5-FU-loaded RBC-coated nanoparticles, respectively. Additionally, the blood half-life of 5-FU-loaded RBC-coated nanoparticles was 29-fold and 18-fold higher than 5-FU solution and 5-FU–chitosan–PLGA nanoparticles, respectively. The mean residence time of 5-FU loaded in 5-FU-RBC-coated nanoparticles increased 25 and 1.5 times, compared to free 5-FU and 5-FU–chitosan–PLGA nanoparticles, respectively.	After 12 h of administration, the amount of 5-FU in the heart decreased by 74%, when comparing the 5-FU-loaded RBC-coated nanoparticles with free 5-FU administration. However, 5-FU-loaded RBC-coated nanoparticles had a pronounced accumulation in the liver and spleen (5.9 and 3.5 μg g^{-1} of 5-Fu, respectively), being the amount of 5-FU 34% higher compared to the amount of free 5-FU. Also, the liver and spleen accumulation of RBC-coated nanoparticles was higher than 5-FU–chitosan–PLGA nanoparticles (2.6 and 2.7 μg g^{-1} of 5-FU).	[130]

(*Continued*)

Table 1. (Continued).

Cell source	Nanoparticle core	Size [nm]	Charge [mV]	Cargo	Vesicles production/coating methodology	Circulation time	Biodistribution	Refs.
	Polypyrrole (PPy)	119.6	−28.2	N.A.	Isolation from mice Vesicles production: physical process → centrifugation Coating: sonication	After 2 h of administration, only 3% ID g^{-1} of bare PPy nanoparticles were detected in the blood. However, the PEGylation of PPy nanoparticles resulted in blood retention of 4% ID g^{-1} after 24 h of administration. After intravenous administration, 10% and 7% ID g^{-1} of PPy@RBC nanoparticles remained in the blood at 24 and 48 h, respectively.	The cell uptake assay at 0.5 and 1 h in RAW264.7 cells showed that PPy nanoparticles presented the highest uptake by macrophages, followed by PEGylated PPy nanoparticles, and biomimetic PPy@RBC nanoparticles. After 2 h of administration, the PPy@RBC nanoparticles combined with the endothelin A receptor antagonist BQ123 (induce tumor vascular relaxation and increase blood flow perfusion) had the highest tumor accumulation, which was 1.37-fold higher than PPy@RBC nanoparticles alone.	[131]
	PLGA	290	−10.8	PFC	Isolation from mice Vesicles production: physical process → centrifugation → sonication Coating: stirring	PFC@PLGA-RBC nanoparticles exhibited a prolonged blood circulation (about 13.93 h), which was higher than bare PFC@PLGA nanoparticles, and also two times higher than the previously reported PFC-coated albumin.	N.D.	[132]
	Poly(caprolactone) (PCL) Membrane modification with iRGD	147.9 (PDI = 0.184)	−16.1	Paclitaxel (PTX)	Isolation from BALB/c mice Vesicles production: physical process → centrifugation → sonication → extrusion Coating: extrusion	After 24 h of administration, RBC-coated nanoparticles presented enhanced plasma concentration of PTX (1.4 ± 0.2 μg mL^{-1}), which was 9.9-fold higher than bare nanoparticles. The blood elimination half-time of RBC nanoparticles was 32.8 h, which was 5.8- and 16.9-fold higher than that of bare nanoparticles and Taxol, respectively.	In vitro studies revealed that the RBC coating reduced the internalization of nanoparticles in mouse macrophages (RAW264.7 cells) by 59%. The RBCs/iRGD nanoparticles presented 5.59-, 2.89-, and 3.02-fold higher tumor accumulation, after 24 h of administration, than bare, bare/iRGD, and RBC-coated nanoparticles, respectively. RBCs/iRGD showed 4.2-, 3.7-, and 1.5-fold higher lung accumulation than bare, bare/iRGD, and RBC-coated nanoparticles, respectively.	[119]

(*Continued*)

Table 1. (Continued).

Cell source	Nanoparticle core	Size [nm]	Charge [mV]	Cargo	Vesicles production/coating methodology	Circulation time	Biodistribution	Refs.
	Prussian Blue membrane modification with hyaluronic acid (HA)	140	−12.16	Gamabufotalin (CS-6)	Isolation from mice or human Vesicles production: physical process → centrifugation → sonication → extrusion Coating: stirring	RBC coating prolonged the nanoparticles' circulation time by 10 h and improved the immune evasion by more than 60%. Furthermore, studies in tumor-bearing BALB/c-nude mice demonstrated that the inclusion of RBC membranes and HA (H-RPC) improved the nanoparticles' half-life by 3.3-fold compared with bare nanoparticles (PC) (7.5 h vs 2.3 h).	Uptake studies with MDA-MB-231 cells revealed that H-RPC nanoparticles presented 1.67-fold higher fluorescence intensity than nanoparticles only coated with RBC vesicles (RPC), after 4 h. The H-RPC nanoparticles' accumulation in tumor tissues was fourfold higher than the PC nanoparticles and ≈1.2 times higher than RPC nanoparticles, at 48 h of treatment.	[133]
	Albumin Membrane modification with cRGD	167 (PDI = 0.332)	−12.8	ICG / 1,2-diaminocyclohexane-platinum (II)	Isolation from BALB/c mice Vesicles production: physical process → centrifugation → extrusion Coating: sonication → extrusion	After 24 h of administration, the blood concentrations of RBC@BPtI and cRGD modified nanoparticles (R-RBC@BPtI) were about 17% and 16% ID g^{-1} at 24 h, whereas decreased to 6% ID g^{-1} for bare nanoparticles.	After 6 h of incubation, R-RBC@BPtI nanoparticles presented higher (2.1 and 1.5 times higher) internalization in B16F10 cancer cells than bare or RBC@BPtI nanoparticles, respectively. Both RBC-coated nanoparticles presented 3.5-fold lower uptake by macrophages than bare nanoparticles. After 24 h of administration, R-RBC@BPtI presented the highest tumor accumulation followed by RBC@BPtI and bare nanoparticles. The accumulation of RBC-coated formulations in the spleen and liver was lower than that of bare nanoparticles.	[134]

(*Continued*)

Table 1. (Continued).

Cell source	Nanoparticle core	Size [nm]	Charge [mV]	Cargo	Vesicles production/coating methodology	Circulation time	Biodistribution	Refs.
	Graphene oxide quantum dots/TAT peptide Membrane modification with DSPE–PEG–RGD	70	−19.11	CS-6/DOX (doxorubicin)	Isolation from BALB/c mice or human Vesicles production: physical process → centrifugation → sonication → extrusion Coating: stirring → sonication	The half-life of Cy5.5, G-Cy5.5, and RBC-coated nanoparticles (G-Cy5.5@M-R) was 1.5, 3, and 4.5 h, respectively. Also, the half-life of G-Cy5.5@M-R nanoparticles in the BALB/c mice increased 1.5-fold compared with bare G-Cy5.5 nanoparticles (3 h vs 4.5 h).	The RGD-modified RBC membranes increased 2.7 and 1.5-fold the uptake by MDA-MB-231 cells, when compared with bare and RBC-coated nanoparticles, respectively. G-Cy5.5 nanoparticles were detected and accumulated in the brain, 12 h after administration. The G-Cy5.5@M-R nanoparticles presented the lowest liver accumulation. After 48 h, most of the G-Cy5.5@M-R nanoparticles were accumulated in the tumor sites and presented a twofold higher fluorescence signal than the G-Cy5.5 nanoparticles.	[135]
Platelet	PEGylated Fe_3O_4 (MNs)	≈100	≈−28	N.A.	Isolation from mice Vesicles production: centrifugation → physical process → sonication → extrusion Coating: stirring → extrusion	The PLT-MNs and RBC-MNs showed a similar blood circulation time, i.e., over 48 h. After 24 h, the blood retention of PLT-MNs and RBC-MNs was ≈13% and ≈11% ID g^{-1}, whereas this value decreased for MNs nanoparticles, ≈5% ID g^{-1}.	Both cell-coated nanoparticles presented ≈2 times lower uptake by macrophages than MNs nanoparticles. After 24 h of incubation, the PLT-MNs showed a ≈7 times higher uptake by MCF-7 cells when compared to RBC-MNs or MNs nanoformulations. After 48 h of nanoparticles administration, PLT-MNs nanoparticles exhibited significantly higher accumulation in the tumor site (≈1.7 times higher than RBC-MNS), and both PLT-MNs and RBC-MNs had lower accumulation in RES organs than MNs nanoparticles. The PLT-MNs resulted in no noticeable increase in IgM and IgG levels, contrasting with the ≈5-fold increase detected for MNs nanoparticles.	[104]

(*Continued*)

Table 1. (Continued).

Cell source	Nanoparticle core	Size [nm]	Charge [mV]	Cargo	Vesicles production/coating methodology	Circulation time	Biodistribution	Refs.
	Polymeric Membrane modification with TRAIL (TNF-related apoptosis-inducing ligand)	120.9	−21.3	DOX	Isolation from mice Vesicles production: centrifugation → physical process → sonication Coating: stirring	Platelet nanoparticles (PM-NV) nanoparticles presented an increase in blood elimination half-life from 5.6 ± 1.4 to 32.6 ± 2.7 h when compared with bare nanoparticles.	PM-NV nanoparticles presented a lower macrophage uptake, ≈4 times lower than bare nanoparticles. After 48 h of administration, the fluorescence intensity of TRAIL-PM-DOX-NV nanoparticles at the tumor site was 1.9-fold higher than nanoparticles without platelet coating (TRAIL-DOX-NV). The TRAIL-PM-DOX-NV nanoparticles presented 3.0- and 4.5-fold higher fluorescence in tumors than that observed on the liver and kidney, respectively.	[136]
	Melanin Membrane modification with RGD	85.92 ± 6.28	−23.5 ± 2.6	DOX	Isolation from mice Vesicles production: physical process → centrifugation Coating: sonication and extrusion	The platelet (NPVs) coating increased five times the blood half-life of the nanoformulations, from 5.13 ± 2.61 to 27.6 ± 4.1 h (NPVs@MNPs/DOX) and 26.4 ± 3.2 h (RGD-NPVs@MNPs/DOX). The mean residence time of nanoparticles was 34.62 ± 5.71, 36.89 ± 7.46, and 7.79 ± 3.23 h, for RGD-NPVs@MNPs/DOX, NPVs@MNPs/DOX, and bare NLVs@MNPs/DOX nanoparticles, respectively.	After 4 h of incubation, RGD-NPVs@MNPs/DOX had a 67.5% reduction in macrophages RAW264.7 uptake, when compared with bare formulation (NLVs@MNPs/DOX). The platelet coating reduced the nanoparticles' accumulation in RES major organs and increased the tumor accumulation, whereas bare nanoparticles (NLVs@MNPs/DOX) accumulated primarily in RES organs. The RGD-NPVs@MNPs/DOX nanoparticles presented the highest tumor accumulation and had a gradual accumulation in the tumor tissue during the 24 h postinjection (≈4.6 times higher than the fluorescence observed at 2 h of administration).	[107]

(*Continued*)

Table 1. (Continued).

Cell source	Nanoparticle core	Size [nm]	Charge [mV]	Cargo	Vesicles production/coating methodology	Circulation time	Biodistribution	Refs.
	$W_{18}O_{49}$	115	N.D.	Metformin	Isolation from human Vesicles production: physical process > sonication Coating: sonication → stirring	N.D.	Platelets-coated nanoparticles (PM-$W_{18}O_{49}$) showed ≈4 and 2 times higher tumor accumulation than bare and PEGylated $W_{18}O_4$ nanoparticles, respectively. The PM-$W_{18}O_{49}$ showed the highest tumor accumulation at 8 h after administration, with a gradual decrease until 24 h. The PM-$W_{18}O_{49}$ nanoparticles presented reduced RES accumulation when compared with bare and PEGylated nanoparticles, during the 24 h of the study.	[137]
	PLGA	98.2 (PDI = 0.118)	−26.76 ± 4.21	Docetaxel (DTX)	Isolation from mice Vesicles production: centrifugation → physical process → sonication → extrusion Coating: sonication → extrusion	N.D.	After 4 h of administration, free DTX was rapidly distributed in tumors (≈120 ng g^{-1}) and was rapidly eliminated at 12 h (≈50 ng g^{-1}), with negligible amounts detected after 24 h of administration. The PLGA/DTX and platelet coated (PM/PLGA/DTX) nanoparticles reached the maximum accumulation at 12 h post-injection (≈200 and ≈400 ng g^{-1} of DTX, respectively). The DTX concentration in tumors was ≈2 times higher, at 24 and 48 h after administration, for PM/PLGA/DTX nanoparticles when compared to PLGA/DTX group.	[138]
Cancer cell	PLGA-DSPE-PEGylated Cell-derived vesicles: MCF-7 cells	200.4	N.D.	ICG	In vitro culture Vesicles production: physical process → extrusion Coating: extrusion	After 24 h of administration, the ICG blood concentration when loaded in cancer cell-coated nanoparticles (ICNPs) was 7–14 times higher than free ICG. Also, the AUC_{24h} of ICNPs was superior to that of the free ICG, 24 h after administration, increasing from 35 to 411 µg min^{-1} mL^{-1}.	Cell-type-specific uptake by ICNPs: 2 times higher in MCF-7 cells than in A549 or MDA-MB-231 cell lines. The ICNPs presented a reduced uptake in RES organs, as well as 3.1 and 4.75-fold increased tumor accumulation at 24 h, when compared with bare nanoparticles and free ICG, respectively. The amount of ICNPs accumulated in the liver and the kidneys was 51% and 34% lower than bare nanoparticles, respectively.	[113]

(*Continued*)

Table 1. (Continued).

Cell source	Nanoparticle core	Size [nm]	Charge [mV]	Cargo	Vesicles production/coating methodology	Circulation time	Biodistribution	Refs.
	Poly(caprolactone) and pluronic copolymer F68 Cell-derived vesicles: 4T1 cells	175.4 ± 0.6	−18.2 ± 0.7	PTX	In vitro culture Vesicles production: physical process → centrifugation → sonication > extrusion Coating: extrusion	The blood half-life of Taxol, bare nanoparticles (PPNs), and cancer cell coated nanoparticles (CPPNs) was 2.5 ± 0.1, 5.9 ± 0.3, and 11.8 ± 0.4 h, respectively. Also, the AUC (0-∞), of Taxol, PPNs, and CPPNs was 8.2 ± 0.8, 23.8 ± 2.4, and 76.2 ± 11.7 mg h^{-1} L^{-1}, respectively. In fact, the AUC (0-∞) and blood half-life of CPPNs were 3.2- and 2.0-fold higher than bare nanoparticles, respectively.	The accumulation of CPPNs in the tumor tissues increased during the first 8 h, and then gradually decreased over time. The PTX concentration in the tumors treated with CPPNs after 8 and 24 h was 4.3- and 2.7-fold higher than that of bare nanoparticles, respectively. The CPPNs' accumulation in the lung (metastases) was 3.7-, 3.5-, and 2.0-fold higher than that of bare nanoparticles, after 4, 8, and 24 h of administration, respectively.	[105]
	PLGA–PEG Cell-derived vesicles: MDA-MB-831	70 ± 4	−20 ± 4	IR780-I/DOX	In vitro culture Vesicles production: physical processes → centrifugation → extrusion Coating: extrusion	N.D.	The cancer cell-coated nanoparticles (CCNP) showed higher uptake by MDA-MB-831 cells than bare nanoparticles. The CCNP nanoparticles showed a slightly higher accumulation in all organs at 24 h, when compared with bare nanoparticles, which started reducing thereafter till 120 h. The CCNP nanoparticles presented a twofold higher fluorescence intensity in the brain and lungs than that of bare nanoparticles, 48 h after administration. The CCNP nanoparticles presented a fluorescence intensity in the spleen similar to the bare nanoparticles at 24 h, which increase by 2.5/3-fold from 24 to 48 h.	[139]

(*Continued*)

Table 1. (Continued).

Cell source	Nanoparticle core	Size [nm]	Charge [mV]	Cargo	Vesicles production/coating methodology	Circulation time	Biodistribution	Refs.
	Mesoporous organosilica Cell-derived vesicles: 4T1 cells	≈110	≈ -20	DOX	In vitro culture Physical process → centrifugation → extrusion Coating: sonication → extrusion	4T1 cells-coated nanoparticles presented ≈3 times higher blood half-life when compared to bare nanoparticles, i.e., 18.4 and 6.6 h, respectively.	The in vitro studies revealed that the 4T1-coated nanoparticles (CM@MON@DOX) presented higher internalization in 4T1 cells and simultaneously reduced the uptake by MCF-10A human breast epithelial cells and RAW264.7 macrophages. In contrast, bare nanoparticles presented reduced uptake by 4T1 cells (when compared with CM@MON@DOX nanoparticles), presenting the highest uptake by RAW264.7 macrophages. The CM@MON@DOX nanoparticles had the highest tumor accumulation (≈2 times higher than bare nanoparticles 12 h post-injection), and the lower uptake by RES organs when compared with bare nanoparticles, respectively (liver: ≈30% ID g^{-1} vs ≈40% ID g^{-1}; spleen: ≈ 10% ID g^{-1} vs ≈20% ID g^{-1}).	[116]

(*Continued*)

Table 1. (Continued).

Cell source	Nanoparticle core	Size [nm]	Charge [mV]	Cargo	Vesicles production/coating methodology	Circulation time	Biodistribution	Refs.
	Mesoporous silica nanospheres and nanorods Cell-derived vesicles: BxPC-3 cells	CM@nanorods: 133.1 ± 5.75 CM@nanospheres: 133.9 ± 10.6	CM@nanorods: −20.8 ± 2.70 CM@nanospheres: −20.4 ± 2.67	DOX	In vitro culture Vesicles production: sonication → physical process → centrifugation Coating: sonication → extrusion	After 24 h of administration, the blood retention of CM@nanorods was ≈20%, which was ≈4 and ten times higher than the retention amount of liposome-coated nanoparticles and bare mesoporous nanoparticles, respectively. Also, CM@nanospheres presented relatively reduced blood circulation when compared with CM@nanorods.	Both CM@nanorods and CM@nanospheres exhibited more effective cellular uptake in BxPC-3 cells than in HPSCs cells. CM@nanorods presented rapid extracellular matrix (ECM) penetration (8.2-fold higher than CM@nanospheres). The accumulation in BxPC3 cells of CM@nanorods was 24.5-fold higher than its spherical counterparts, after 4 h of incubation. After 8 h, the fluorescence of CM@nanorods was detected at the tumor site and increased gradually. Bare nanorods and nanospheres presented the lowest tumor accumulation during the procedure, followed by liposome-coated nanoformulations and CM@nanospheres.	[140]
	3 models of mesoporous silica (MSN0, MSN1, MSN2) Cell-derived vesicles: HeLa cells	≈200	≈−30	Cytotoxic ribonuclease A (RNase A)	In vitro culture Vesicles production: physical process → sonication → extrusion Coating: sonication → extrusion	The elimination half-times of cancer cell-coated MSN0@RNaseA@CM (16.9 h), MSN1@RNaseA@CM (20.1 h), and MSN2@RNaseA@CM (15.2 h), which were 1.8-, 2.1-, and 2.0 times higher than those of uncoated formulations: MSN0@RNaseA (9.4 h), MSN1@RNaseA (9.7 h), and MSN2@RNaseA (7.5 h), respectively.	MSN@RNaseA@CM formulations presented increased internalization by HeLa cells than MCF-7 cells. Also, the cancer cell coating increased the uptake by HeLa cells and significantly reduced the nanoparticles uptake by RAW264.7 cells, compared with bare nanoparticles. Also, no difference in cellular internalization was observed among the three types of MSNs@-RNaseA with or without the cancer cell membrane coating. After 24 h, all nanoformulations were trapped in the liver and spleen, with the MSNs@RNase@CM formulations showing an enhanced tumor accumulation and reduced spleen retention, when compared with bare counterparts.	[117]

(*Continued*)

Table 1. (Continued).

Cell source	Nanoparticle core	Size [nm]	Charge [mV]	Cargo	Vesicles production/coating methodology	Circulation time	Biodistribution	Refs.
	Janus magnetic mesoporous organosilica Cell-derived vesicles: MCF-7 and 4T1 cells	≈300	≈−20	Chlorine e6 (Ce6)	MCF-7 cells: in vitro culture Vesicles production: physical process → centrifugation → extrusion → sonication 4T1 cells: in vitro culture Vesicles production: physical process → centrifugation → extrusion → sonication Coating: sonication → coextrusion	The blood circulation half-life of cell membrane-coated nanoparticles (CM@M-MON@Ce6) (5.6 h) was 4.7 times greater than that of bare nanoparticles (M-MON@Ce6) (1.2 h).	In vitro studies revealed that M-MONs and CM@M-MONs nanoparticles presented increased fluorescence intensity in both MCF-7 and MCF-10A cells, while they showed decreased signals in macrophages. The CM@M-MON nanoparticles had higher fluorescence intensity in MCF-7. Both formulations presented higher accumulation in the liver and spleen, however, these values were inferior in the CM@M-MONs group. The CM@M-MONs presented almost 4 times higher tumor accumulation than bare nanoparticles (M-MONs).	[126]
	Gold nanocages (AuNCs) Cell-derived vesicles: H22 cells	104.5	−30.5	DOX	In vitro culture Vesicles production: physical process → sonication → centrifugation Coating: extrusion	The AUC (0-∞) of both cancer cell coated nanoformulations (CAuNCs and DOX@CAuNCs) was about 2.1-fold higher than that of bare nanoparticles. The terminal elimination half-life (t1/2β) of CAuNCs (35.82 h) and DOX@CAuNCs (34.02 h) was ≈1.8- and 1.7-fold higher than that of AuNCs nanoparticles (20.06 h).	Both cancer cell-coated nanoparticles presented ≈3-fold higher H22 cellular uptake than bare nanoparticles, after 4 h of incubation. The bare nanoparticles presented a ≈3-fold higher uptake by RAW264.7 macrophages than CAuNCs and DOX@CAuNCs nanoparticles. After 48 h of administration, CAuNCs and DOX@CAuNCs nanoparticles were accumulated in tumors 1.9- and 2.0 times higher than AuNCs nanoparticles. Also, nanoformulations were highly accumulated in the liver, lung, and spleen however, such was more pronounced in AuNCs.	[109]

(*Continued*)

Table 1. (Continued).

Cell source	Nanoparticle core	Size [nm]	Charge [mV]	Cargo	Vesicles production/coating methodology	Circulation time	Biodistribution	Refs.
	Self-assembled nanodrug (DOX/Ber) Cell-derived vesicles: 4T1 cells	≈150	≈−25	DOX/Berberine (Ber)	In vitro culture Vesicles production: physical process → centrifugation → extrusion → sonication Coating: sonication → extrusion	Cell-coated nanoparticles (DBNP@CM) presented a longer blood elimination half-life, 6.3 h) than bare DBNP (2.4 h) and free DOX (1.5 h).	The flow cytometry analysis showed that the fluorescence intensity of DOX in DBNP@CM-treated 4T1 cells was ≈2-fold higher than that of DBNP-treated cells. The DBNP@CM nanoparticles presented 2 times lower uptake by RAW264.7 macrophages than DBNP nanoparticles. The accumulation of Ber and DOX in RES organs for DBNP@CM group was lower than in bare nanoparticles. Also, DBNP@CM nanoparticles presented a preferential accumulation in tumor tissue (≈4 times higher) than DBNP nanoparticles.	[141]
	Bismuth (Bi)/DSPE-PEG Cell-derived vesicles: CT26 cells	≈50 ± 2	−22.6 ± 1.7	N.A.	In vitro culture Vesicles production: physical process → sonication → centrifugation Coating: extrusion	Cancer cell-coated nanoparticles (Bi@CCM) exhibited almost ≈2.9 times higher blood circulation half-life (11.5 h) than those of PEGylated Bi nanoparticles (4.0 h). The PEGylated Bi nanoparticles concentration in mice blood decreased rapidly from 43.15 ± 1.53% ID g^{-1} at 0.5 h to 1.84 ± 0.69% ID g^{-1} at 16 h, stabilizing in the 1.40 ± 0.95% ID g^{-1} after 24 h. The Bi concentration of Bi@CCM in blood decreased slowly from 53.30 ± 3.34% ID g^{-1} at 0.5 h to 12.88 ± 2.32% ID g^{-1} at 24 h. After 24 h of administration, the remained Bi concentration of Bi@CCM group (12.88 ± 2.32% ID g^{-1}) was 9.2-fold higher than that of the PEGylated Bi group (1.40 ± 0.95% ID g^{-1}).	The Bi@CCM nanoparticles exhibited a relatively higher Bi uptake by CT26 cells (1.2-fold) when compared to PEGylated Bi nanoparticles, after 12 h of incubation. Bi@CCM exhibited higher tumor accumulation (4.7 ± 0.56% ID g^{-1}, ≈2.3 times) than PEGylated Bi nanoparticles (2.03 ± 0.60% ID g^{-1}). The PEGylated Bi nanoparticles presented a Bi concentration of 0.94 ± 0.04% ID g^{-1} in the liver, 5.99 ± 0.53% ID g^{-1} in the spleen, 3.47 ± 0.15% ID g^{-1} in the lung, and 7.74 ± 0.80% ID g^{-1} in the kidney, respectively. In contrast, the Bi@CCM nanoparticles presented less accumulation in the above-described organs (e.g., 2.36 ± 0.24% ID g^{-1} in the liver and 1.66 ± 0.19% ID g^{-1} in the spleen).	[142]

(*Continued*)

Table 1. (Continued).

Cell source	Nanoparticle core	Size [nm]	Charge [mV]	Cargo	Vesicles production/coating methodology	Circulation time	Biodistribution	Refs.
Immune cell	Gold nanoshell (AuNSs) Cell-derived vesicles: macrophages	≈100	−20.8	N.A.	In vitro culture Vesicles production: physical process → centrifugation → sonication → extrusion Coating: sonication → extrusion	After 48 h of administration, more than 30% of macrophages-coated nanoparticles (MPCM-AuNSs) were present in blood vessels. However, bare AuNSs were almost eliminated from the blood after 24 h of administration.	After 48 h, 7.48% ID g^{-1} of MPCM-AuNSs were accumulated in the tumor tissue, contrasting with the 1.61% ID g^{-1} of bare nanoparticles. The MPCM-AuNSs also presented lower uptake by RES organs, compared with bare nanoparticles.	[143]
	Albumin Cell-derived vesicles: macrophages	188.7 ± 4.8	−10.5	PTX	In vitro culture Vesicles production: physical process → centrifugation → extrusion Coating: extrusion	After 24 h of administration, macrophage-coated nanoparticles (RANPS) displayed higher fluorescence intensity in blood than bare nanoparticles.	The RANPS uptake by the B16F10 cells was 3.41-, 4.3-, and 5.88 times higher than that of bare nanoparticles after 0.5, 1, and 2 h, respectively. The RANPS presented higher tumor accumulation and lower retention in the spleen and lung than bare nanoparticles, after 24 h of administration.	[144]
	DNA tetrahedron dendrimer and N-(p-maleimidobenzoyl) dipalmitoyl phosphoethanolamine Cell-derived vesicles: macrophages	91.0	−22.6	DOX	In vitro culture Vesicles production: physical process → sonication → centrifugation Coating: extrusion	N.D.	The DOX-MPK@MDL nanoparticles presented higher internalization into 4T1 cells than bare nanoparticles, being the DOX mainly accumulated in the cells' nucleus 4 h after administration. The fluorescence signal in the lungs of DOX-MPK@MDL nanoparticles gradually increased after 1 h and reached its maximum at 4 h, and was superior to that of bare nanoparticles. Moreover, after the establishment of 4T1-luc tumors and lung metastasis in BABL/c nude mice, the DOX-MPK@MDL nanoparticles presented a 2.1-fold higher fluorescence intensity in the lungs than bare nanoparticles, at 4 h postinjection.	[118]

(*Continued*)

Table 1. (Continued).

Cell source	Nanoparticle core	Size [nm]	Charge [mV]	Cargo	Vesicles production/coating methodology	Circulation time	Biodistribution	Refs.
	Fe_3O_4 Cell-derived vesicles: macrophages	≈100 nm	≈−18	N.A.	In vitro culture Vesicles production: physical process → disruption (using a dounce homogenizer) → centrifugation → extrusion Coating: extrusion	RBC-coated (Fe_3O_4@RBC) and macrophages-coated (Fe_3O_4@MM) nanoparticles presented similar blood retentions, which were ≈2 times higher than bare nanoparticles, from 8 to 48 h of administration.	Fe_3O_4, Fe_3O_4@RBC, and Fe_3O_4@MM nanoparticles were incubated with RAW264.7 cells for 24 h, and both cell-coated nanoformulations presented reduced macrophages' uptake (≈2 times lower) than bare Fe_3O_4 nanoparticles. The Fe_3O_4@MM nanoparticles showed higher tumor accumulation (≈2 and threefold higher than Fe_3O_4@RBC and bare nanoparticles, respectively) and lower retention in the spleen and liver than Fe_3O_4@RBC and bare nanoparticles.	[112]
	PEG–PLGA Cell-derived vesicles: neutrophil	167.4 ± 2.6 (PDI = 0.215)	−14.5 ± 1.1	Celastrol	Isolated from rats Vesicles production: extrusion Coating: extrusion	Neutrophil-coated nanoparticles presented extended circulation time ($t_{1/2}$ = 2.899 ± 0.699 h) and C_{max} (980 ± 100.233 µg L^{-1}), when compared to bare nanoparticles ($t_{1/2}$ = 2.352 ± 0.141 h) (C_{max} = 600 ± 56.781 µg L^{-1}), respectively.	Neutrophil-coated nanoparticles presented remarkably higher accumulation at the tumor site than bare nanoparticles after 24 h. However, both formulations presented high liver accumulation 24 h after administration.	[145]
	PLGA Cell-derived vesicles: neutrophil	94.8 ± 7.6 (PDI = 0.13 ± 0.03)	−34.2 ± 3.3	Carfilzomib	Isolated from mice Vesicles production: centrifugation → physical process → centrifugation Coating: Sonication	The half-life of bare, neutrophil-coated nanoparticles, and PEGylated-PLGA nanoparticles were 0.77, 6.59, and 4.73 h, respectively. The AUCs of PEGylated-PLGA and neutrophil-coated nanoparticles were 134.4 and 207.2-fold higher than that of bare nanoparticles.	After 24 h of administration, the neutrophil-coated nanoparticles showed an accumulation in lung metastatic foci 2.12- and 3.02-fold higher than that of bare and PEGylated-PLGA nanoparticles, respectively.	[122]

(*Continued*)

Table 1. (Continued).

Cell source	Nanoparticle core	Size [nm]	Charge [mV]	Cargo	Vesicles production/coating methodology	Circulation time	Biodistribution	Refs.
	mPEG-PLGA Cell-derived vesicles: natural killer (NK)	85 ± 1.2 (PDI = 0.105)	−11.8 ± 0.8	4,4′,4″,4‴-(Porphine-5,10,15,20-tetrayl) tetrakis (benzoic acid) (TCPP)	Isolation from BALB/c mice Vesicles production: centrifugation → culture → physical process → centrifugation Coating: extrusion	The NK nanoparticles presented a blood half-life of 8 h, whereas in bare nanoparticles this value was 5.5 h.	NK-TCPP nanoparticles' fluorescence intensity on cancer cells was five times higher than that obtained with bare nanoparticles and 32 times stronger than in normal cells. In vivo studies showed that NK nanoparticles accumulated in the tumor tissue during the first 24 h and then gradually decrease with time, showing a six times higher accumulation in 4T1 tumors than bare nanoparticles.	[146]
	PLGA Cell-derived vesicles: T cell modified with N_3 (N_3-TINPs)	≈75	N.D.	ICG	Isolated from humans and expanded in vitro Vesicles production: physical process → sonication → centrifugation → extrusion Coating: extrusion	The N_3-TINPs treated group presented a higher ICG concentration in the blood, 15 min postinjection than bare nanoparticles (INPs). The AUC_{24h} of N_3-TINPs nanoparticles (360 µg min mL^{-1}) was fourfold higher than that detected of INPs (84 µg min mL^{-1}).	In vitro studies show that Raji cancer cells treated with N_3-TINPs had a higher ICG fluorescence than that observed in cells treated with TINPs (≈1.3 times higher), INPS (≈2.2 times higher), and free ICG (≈3.5 times higher). After 48 h, the N_3-TINPs treated group presented ≈30 and ≈50% higher fluorescence intensity in tumors than that obtained in mice treated with TINPs and INPs, respectively.	[147]

(*Continued*)

Table 1. (Continued).

Cell source	Nanoparticle core	Size [nm]	Charge [mV]	Cargo	Vesicles production/coating methodology	Circulation time	Biodistribution	Refs.
Hybrid	Melanin Cell-derived vesicles: (RBC/MCF-7 at different membrane protein weight ratio (RBC:MCF-7, 1:0, 2:1, 1:1, 1:2, and 0:1)	240	−31.1 ± 0.8	N.A.	RBC: isolated from BALB/c mice Vesicles production: physical process → centrifugation → extrusion MCF cells: in vitro culture Physical process → centrifugation Coating: Sonication → coextrusion	After 24 h of administration, melanin@RBC-MCF-7 in the 1:1 and 2:1 groups presented a blood retention of 14.46 ± 1.45 and 15.74 ± 0.53% ID g^{-1}, respectively, which was similar to the 1:0 group (16.43 ± 0.77% ID g^{-1}). The melanin@RBC-MCF-7 in the 1:2 and 0:1 groups presented lower blood retentions of 8.90 ± 1.99% and 5.19 ± 2.18% ID g^{-1}, respectively, followed by bare melanin nanoparticles 2.23 ± 1.05% ID g^{-1}.The circulation half-life of melanin@RBC-MCF-7 nanoparticles, with 1:0, 2:1, 1:1, 1:2, and 0:1 ratios, was 11.2, 10.9, 10.7, 8.4, and 5.1 h, respectively, whereas for bare nanoparticles this value was 4.0 h.	The melanin@RBC-MCF-7 nanoparticles exhibited significantly higher uptake in MCF-7 cells at 24 h of incubation, when compared with 4T1, MCF-10A, and RAW264.7 cells. The increase in the MCF-7 membrane ratio in the hybrid membrane enhanced the uptake by MCF-7 cells. After 4 h of administration, hybrid nanoparticles in 1:1 group presented 1.52-, 1.27-, 2.01-, 2.52-, and 4.14-fold higher tumor accumulation than 1:0, 2:1, 1:2, 0:1, and 0:0 groups. All groups exhibited similar liver and spleen accumulations, however, in the 1:2, 1:1, 2:1, and 1:0 groups occurred a gradual reduction in liver retention (30.95 ± 1.77%, 29.8 ± 1.32%, 29.14 ± 1.55%, and 28.16 ± 1.25% ID g^{-1}), which was lower than in 0:1 (34.02 ± 2.13% ID g^{-1}) and 0:0 groups (35.52 ± 2.4% ID g^{-1}).	[148]
	Copper sulfide (CuS) Cell-derived vesicles: (RBC/B16-F10)	≈210	−23	DOX	RBC: Isolated from BALB/c mice Vesicles production: physical process → centrifugation B16-F10 cells: in vitro culture Vesicles production: physical process → centrifugation Coating: sonication	After 24 h postinjection, the hybrid (CuS@[RBC–B16]) nanomaterials presented a blood retention of 20.2% ID g^{-1}, slightly lower than that of RBC-coated (CuS@RBC; 22.9% ID g^{-1}) and higher than that of B16-F10-coated (CuS@B16; 14.5% ID g^{-1}), and bare (CuS; 5.2% ID g^{-1}) nanoparticles. The blood circulation half-life of CuS@[RBC−B16] and CuS@RBC nanoparticles was 9.6 and 9.9 h, respectively, whereas this value decreased to 6.0 h for CuS@B16 and 1.0 h for bare nanoparticles.	The hybrid nanoparticles presented 8.25- and 9.78 times higher internalization in B16-F10 cancer cells than in HT1080 or NHDF cells, after 4 h of incubation. The in vivo studies also demonstrated that hybrid nanoparticles had 1.5-, 1.4-, and 2.5-fold higher tumor accumulation than CuS@RBC, CuS@B16, and bare nanoparticles, respectively. The accumulation in the spleen and liver was 34.6% and 23% lower in hybrid nanoparticles than in bare nanoparticles, respectively.	[149]

(*Continued*)

Table 1. (Continued).

Cell source	Nanoparticle core	Size [nm]	Charge [mV]	Cargo	Vesicles production/coating methodology	Circulation time	Biodistribution	Refs.
	PLGA Cell-derived vesicles: (PTL/RBC)	≈100	≈−25	N.A.	RBC: Isolated from human PTL: Isolated from human Vesicles production: both cell membranes were mixed and stirred Coating: Sonication	RBC, PTL, and [RBC-PTL]-coated nanoparticles had one-phase half-lives of 5.7, 5.7, and 6.4 h, and two-phase elimination half-lives of 42.4, 38.3, and 51.8 h, respectively.	After 24 h of administration, both formulations presented similar accumulation in major organs with the majority of the nanoformulations being detected in the liver and spleen.	[123]
	PLGA/1,2-dioleoyloxy-3-(trimethylammonium) propane (DOTAP) Cell-derived vesicles: (RBC/NCI-H1299 cancer cell)	192.8 ± 8 (PDI = 0.16)	N.D.	Vorinostat (SAHA)	RBC: isolated from BALB/c mice Vesicles productions: physical process → centrifugation NCI-H129 cells: in vitro culture Vesicles productions: physical process → centrifugation; Then, both cell membranes were mixed and sonicated; Coating: coextrusion	The inclusion of hybrid-derived vesicles improved the blood circulation of nanoparticles threefold, when compared to bare nanoparticles. The bare nanoparticles had a 30% decrease in blood after 5 h, and 11% after 24 h of administration. However, 36% of hybrid nanoparticles remained in circulation after 24 h.	CLSM analysis indicated that hybrid nanoparticles show lower cellular uptake by the nonhomologous cells (such as NIH-3 T3, H9C2, and Raw 264.7 cells) when compared with NCI-H1299 cells. The hybrid nanoparticles had stronger fluorescence on metastatic foci, when compared with the bare, RBC-coated, or NCI-H1299-coated nanoparticles. The liver fluorescence in the group treated with hybrid nanoparticles was 5-fold, 2-fold, and 1.3-fold higher than bare, RBC-coated, and NCI-H1299-coated nanoparticles.	[150]
	PLGA Cell-derived vesicles: (macrophages RAW264.7/4T1 cancer cell)	163 ± 9.61	−31.1	DOX	RAW264.7: in vitro culture Vesicles production: physical process → centrifugation 4T1 cells: in vitro culture Vesicles production: physical process → centrifugation Then, both cell membranes were mixed and sonicated Coating: sonication	N.D.	The DPLGA@[RAW-4T1] nanoparticles presented two- to fourfold higher fluorescence intensity in 4T1 cells than in other cell groups. The DPLGA@[RAW-4T1] hybrid nanoparticles presented higher internalization in 4T1 cells (88.70%) than the single-coated counterparts DPLGA@RAW (72.30%) and DPLGA@4T1 (74.23%) nanoparticles. Bare nanoparticles showed higher accumulation in the liver and kidneys but lower retention in the lungs, when compared with DPLGA@[RAW-4T1]. The hybrid nanoparticles showed 5.14-fold higher fluorescence in lung metastasis than that in bare nanoparticles.	[151]

(*Continued*)

Table 1. (Continued).

Cell source	Nanoparticle core	Size [nm]	Charge [mV]	Cargo	Vesicles production/coating methodology	Circulation time	Biodistribution	Refs.
	Liposome Cell-derived vesicles: (immune cell (Murine J774A.1 cells)/HN12 cancer cell)	≈160	−14.4 ± 2.2	PTX	J774A.1 cells: in vitro culture Vesicles production: homogenized → physical process → centrifugation → sonication → extrusion HN12 cells: in vitro culture Vesicles production: homogenized → physical process → centrifugation → sonication → extrusion Coating: sonication → coextrusion	Immune cancer-coated liposomes had a higher half-life (20.2 h), followed by hybrid liposomes (8.1 h), cancer cell-coated liposomes, and control liposomes (4.0 h). The blood retention of immune and cancer-coated liposomes after 48 h was 35%.	Immune cell-coated nanoparticles had a 2.8-fold lower uptake by J774A.1 cells than the liposomes control group. The tumor cell-coated liposomes had a 4.3-fold increase in uptake by HN12 cells, and a 1.6-fold decrease in uptake by J774A.1 cells, when compared to the control group. The incorporation of both leukocyte and tumor cell membrane resulted in 3.9 times higher uptake by HN12 tumor cells and 2.4 times lower uptake by J774A.1 cells. After 48 h of administration, the tumor accumulation of hybrid liposomes increased 9.3-fold to 79.1 ± 6.6% ID g^{-1} when compared with the control liposomes (8.5 ± 3.4% ID g^{-1}). The immune-coated nanoparticles and cancer cell-coated nanoparticles presented 2.7-fold and 4.4-fold higher tumor accumulation than control nanoparticles, respectively. All cell-coated formulations had lower accumulation in the spleen and liver (40–63%), as well as in the lung (29% lower) than that of control liposomes, respectively.	[152]
	Mesoporous gold nanorod Cell-derived vesicles: RBC/cancer cell (HeLa)	≈150	−14.7 ± 1.68	DOX	RBC: isolated from BALB/c miceVesicles production: physical process → centrifugation HeLa: in vitro culture Vesicles production: physical process → centrifugation Then, both cells were mixed and sonicated. Coating: coextrusion	Bare nanoparticles were cleared from the blood circulation within 6 h. The cell membrane coating of RBC, or HeLa cells, or their conjugation increased by 15% the concentration of nanoparticles in the blood at 6 h after administration. Compared to the hybrid nanoparticles, the single RBC-coated nanoparticles presented the highest blood circulation after 24 h, with 15% still being detectable in blood.	Hybrid nanoparticles showed higher photoacoustic imaging (PA) intensity in tumors at different time points with the tumor accumulation following: Hybrid > HeLa-coated > RBC-coated > bare nanoparticles. The PA signal in the tumors increased within 4 h and reached a plateau at 8 h. The fluorescence intensity of bare nanoparticles in the tumor was ≈5 times, 6 times, and 15 times lower than RBC-coated, HeLa-coated, and hybrid-coated nanoparticles, respectively.	[153]

(*Continued*)

Table 1. (Continued).

Cell source	Nanoparticle core	Size [nm]	Charge [mV]	Cargo	Vesicles production/coating methodology	Circulation time	Biodistribution	Refs.
	Zr–metal–organic framework (PCN) Cell-derived vesicles: cancer cell (4T1)/dendritic cells	≈160	≈−30	N.A.	4T1 cells: in vitro culture Dendritic cells: in vitro culture Vesicles production: both cell lines were mixed and stirred → centrifugation → physical process Coating: sonication	N.D.	The tumor accumulation of the nanoformulations occurred in the following order: cancer cell-coated nanoparticles (PCN@CM) > hybrid nanoparticles (PCN@FM) > dendritic cell-coated nanoparticles PCN@DM > bare nanoparticles (PCN). The PCN@CM and PCN@FM presented a higher accumulation in the tumor than in the RES organs, 96 h postinjection. The bare and PCN@DM nanoparticles had higher RES accumulation than in tumor tissue. The PCN@FM and PCN@CM nanoparticles presented a higher uptake by 4T1 cells than by CT26 or 3T3 cells, and both formulations were more readily uptaken by 4T1 cells than PCN@DM nanoparticles.	[154]
	Fe_3O_4 Cell-derived vesicles: RBC/cancer cell (ID8 cells)	≈52	−24	ICG	RBC: isolation from mice Vesicles production: physical process → centrifugation ID8 cells: in vitro culture Vesicles production: physical process → sonication → centrifugation Then, both cells were mixed and sonicated Coating: sonication	After 24 h, the hybrid nanoparticles (Fe_3O_4-ICG@IRM) presented a blood retention of 14.2% ID g^{-1}, whereas single RBC-coated (Fe_3O_4-ICG@RBC-M), single cancer cell-coated (Fe_3O_4-ICG@ID8-M), and bare Fe_3O_4-ICG nanoparticles had blood retentions of 18.6%, 8.7%, and 2.9% ID g^{-1}, respectively. The circulation half-lives of hybrid Fe_3O_4-ICG@IRM and Fe_3O_4-ICG@RBC-M were ≈7.1 and 8.1 h, respectively, which were longer than those for bare Fe_3O_4-ICG (of 2.6 h) and Fe_3O_4-ICG@ID8-M nanoparticles (4.4 h).	After 4 h of incubation, Fe_3O_4-ICG@ID8-M and hybrid Fe_3O_4-ICG@IRM-treated ID8 cells had 8.8- and 5.0-fold higher fluorescence than that recorded in Fe_3O_4-ICG@RBC-M treated cells, respectively. The tumor accumulation of hybrid Fe_3O_4-ICG@IRM was 2.9-fold, 1.8-fold, and 1.5-fold higher than that of bare Fe_3O_4-ICG, Fe_3O_4-ICG@ID8-M, and Fe_3O_4-ICG@RBC-M nanoparticles.	[155]

(*Continued*)

Table 1. (Continued).

Cell source	Nanoparticle core	Size [nm]	Charge [mV]	Cargo	Vesicles production/coating methodology	Circulation time	Biodistribution	Refs.
	PPy Cell-derived vesicles: RBC/PLT	141.1	-26 ± 2	N.A.	RBC: isolation from human Vesicles production: physical process → centrifugation PLT: isolation from human Vesicles production: physical process → centrifugation Then, both cells were mixed and sonicated Coating: coextrusion	After 24 and 48 h of administration, the blood retention of hybrid nanoparticles was 11.5% and 8.9% ID g^{-1}, respectively, which was higher than that of single-coated PLT nanoparticles (3.1% and 1.7% ID g^{-1}).	The administration of hybrid nanoparticles resulted in higher tumor inhibition (average tumor weight 0.136 g), whereas the mice treated with single-coated PLT or RBC nanoformulations presented tumors with 0.346 and 0.420 g, respectively. After 4 h of administration single-coated PLT nanoparticles presented the highest spleen and liver accumulation and a reduced lung accumulation. Similarly, single-coated RBC nanoparticles presented higher accumulation in kidneys than the other nanoformulations.	[156]
	Gold nanocages (GNCs) Cell-derived vesicles: RBC/cancer cell (MCF-7)	≈75	-19.5 ± 0.7	DOX	RBC: in vitro culture Vesicles production: homogenized → sonication → extrusion MCF-7: in vitro culture Vesicles production: homogenized → sonication → extrusion Coating: sonication and coextrusion	N.D.	After 6 h of incubation, the cancer cell-coated (CM-GNC) and hybrid (CM-EM-GNCs) nanoparticles presented a 3.9- and 4.1-fold higher gold signal in MCF-7 cells than in MCF 10A cells, respectively. The hybrid and RBC-coated (RBC-GNC) nanoparticles presented almost four times lower uptake by RAW264.7 macrophages than CM-GNC and bare nanoparticles. Hybrid nanoparticles exhibited a 1.2-, 1.7-, and 2.2-fold higher tumor accumulation than single-coated cancer cell (CM-GNCs@DOX), RBC-coated (RBC-GNCs@DOX), and bare (GNCs@DOX) nanoparticles. The accumulation in the RES organs by hybrid nanoparticles was significantly lower when compared with other nanoformulations.	[157]

Abbreviations: CLSM: confocal laser microscope; CM: cancer membrane; PLT: platelet; RBC: red blood cells; AUC: area under curve.

inlets, merged in the Y-shaped channel, and mixed in the S-shaped channel. The electric pulses between two electrodes in the electroporation zone, promote the penetration of nanoparticles into cell-derived vesicles to obtain the cell-derived vesicles coated nanoparticles in the outlet. Therefore, the process can be optimized by fine-tuning the flow speed as well as the pulse voltage and period.

4.2. Red Blood Cell-Derived Vesicles Camouflage Nanoparticles

Erythrocytes or red blood cells (RBCs) primary function is the transport of oxygen/carbon dioxide in the human body. On average, there are 4.2–6.2 billion of RBCs per mL of blood. They are the main constituent of the blood figurative elements and circulate in the blood for 100–120 days.[108,158] Moreover, during the maturation process, the RBCs lose their nuclei and most of the cytoplasmatic organelles, which already facilitate the extraction and formation of RBC-derived vesicles.[159] After the extraction and purification process, the RBC-derived vesicles still present the original biological properties, due to the preservation of their natural membrane "self-markers" including CD47 proteins, sialic acid moieties, and glycan.[160–162] Particularly, the expression of CD47 proteins on the RBC membranes is pointed out as the main self-marker that is responsible for reducing RES uptake.[108,162] CD47 act as "don't eat me" marker on the RBCs surface, inhibiting the macrophages' phagocytosis through interactions with the signal regulatory protein-alpha (SIRP-α) receptor.[160]

Therefore, RBC-derived vesicles are highly promising surface modifications for prolonging the nanoparticles' circulation time and prompting the escape from immunogenic clearance.[108] RBC-derived vesicles were the first reported cell-derived biomimetic systems for application with nanoparticles, being the most explored so far in the biomedical area. Hu et al. showed one of the first applications of RBC-derived vesicles to camouflage nanoparticles, obtaining a 2.5 times higher elimination half-life when compared to the PEGylated nanoparticles, i.e., an increase from 15.8 to 39.6 h for the RBC-coated nanoparticles.[163] Also, RBC nanoparticles presented a higher blood circulation half-life than PEGylated nanoparticles, 9.6 and 6.5 h, respectively.[163] Rao et al. developed biomimetic Fe_3O_4@RBC nanoparticles and evaluated their pharmacokinetic profile upon repeated injections, and compared the results with PEGylated Fe_3O_4 nanoparticles.[108] After 8 and 24 h of administration, the Fe_3O_4@RBC nanoparticles exhibited a blood retention of 18.3% and 14.2% ID g^{-1}, respectively, whereas these values were substantially smaller, ≈10 and ≈5% ID g^{-1}, for PEGylated nanoparticles. Also, Fe_3O_4@RBC nanoparticles presented lower liver and spleen accumulation (49.2 ± 7.1 and 100.1 ± 16.3 μg g^{-1} tissue) compared with the PEGylated nanoparticles (117.4 ± 30.3 and 174.5 ± 43.7 μg g^{-1} tissue), which demonstrate that the RBC coating can reduce the RES uptake. Furthermore, 5 days after the nanoparticles' first injection, the authors observed similar pharmacokinetics for the second dose of Fe_3O_4@RBC nanoparticles, whereas the PEGylated nanoparticles showed a significant reduction in the blood retention (i.e., Fe content decreased from 5% to 1.8% ID g^{-1}, 24 h after the second injection). Accordingly, the IgG and IgM levels in the mice treated with Fe_3O_4 and Fe_3O_4@PEG were three times higher than the control group (5 days after the second administration), contrasting with the normal levels of the Fe_3O_4@RBC nanoparticles. Therefore, these works demonstrate that RBC-based vesicles through the CD47/SIRP-α signaling pathway can effectively reduce the nanoparticles' immune recognition and improve their pharmacokinetic profile better than PEG-based coatings. Furthermore, Ren et al. developed albumin nanoparticles that encapsulate ICG (indocyanine green – an NIR dye) and perfluorocarbon (PFC), coated with RBC-derived vesicles (IPH@RBC nanoparticles) for application in cancer photodynamic therapy (**Figure 2**).[127] The elimination lifetime of IPH@RBC nanoparticles was 15.71 h, ≈14-fold higher than ICG encapsulated in albumin (ICG-HAS) and bare IPH nanoparticles. Also, it was demonstrated that the RBC-derived vesicles reduced the uptake by RAW264.7 macrophages in ≈50%, when compared with uncoated IPH nanoparticles. The ICG fluorescence analysis on mice's tumors revealed that IPH@RBC nanoparticles have a 5.6-fold higher tumor accumulation than the uncoated IPH nanoparticles, which results in an improved antitumoral effect.

In another work, Ye et al. produced RBC-based vesicles for the delivery of self-assembly small molecular drugs, 10-hydroxycamptothecin (10-HCPT) and ICG.[129] After 24 h of injection, ≈16.3% ID g^{-1} of RBCs@ICG-HCPT nanoparticles were detected in the blood, whereas in the same period only ≈2.0% and 7.5% ID g^{-1} of free ICG and ICG-HCPT nanoparticles were detected, respectively. Moreover, the RBC coating also reduced the accumulation of the nanoparticles in the liver and spleen (≈20% and ≈19% ID g^{-1}, respectively) and increased their accumulation in the tumor (≈8% ID g^{-1}), when compared with ICG-HCPT nanoparticles (with ≈27%, ≈24%, and ≈5% ID g^{-1}, on liver, spleen, and tumor, respectively).

Despite the improved blood circulation and tumor accumulation of RBC camouflaged nanoparticles, it is still crucial to improve the nanoparticles' specificity toward cancer cells. Therefore, different studies have combined the RBC camouflage nanoparticles with different targeting moieties. Liu et al. produced Prussian blue nanoparticles with a hollow porous structure coated with hyaluronic acid-modified RBC-based vesicles (H-RPC), to deliver the photothermal sensitizer CS-6.[133] The results show that RBC coating prolonged the nanoparticles' circulation time by 10 h and improved immune evasion by more than 60%. Uptake studies with MDA-MB-231 cells revealed that H-RPC nanoparticles presented 1.67-fold higher fluorescence intensity than nanoparticles only coated with RBC vesicles (RPC). Furthermore, studies in tumor-bearing BALB/c-nu mice demonstrated that the inclusion of RBC membranes and hyaluronic acid improved the nanoparticles' half-life by 3.3-fold in comparison with PC nanoparticles (7.5 vs 2.3 h). Moreover, the H-RPC nanoparticles' accumulation in tumor tissues was fourfold higher than the PC nanoparticles and ≈1.2 times higher than RPC nanoparticles. Under laser irradiation, the H-RPC-treated group presented a 45.4% and 23.1% higher tumor inhibition than PC- or RPC-treated groups, respectively. Similarly, Su et al. developed RBC mimetic polymeric nanoparticles loaded with anticancer drug paclitaxel (PTX), modified with the tumor penetrating peptide iRGD for the treatment of metastatic breast cancer.[119] RBC mimetic nanoparticles showed enhanced retention of PTX in the blood (elimination half-time of 32.8 h), contrasting with the 5.6 h obtained for the parental PTX-polymeric

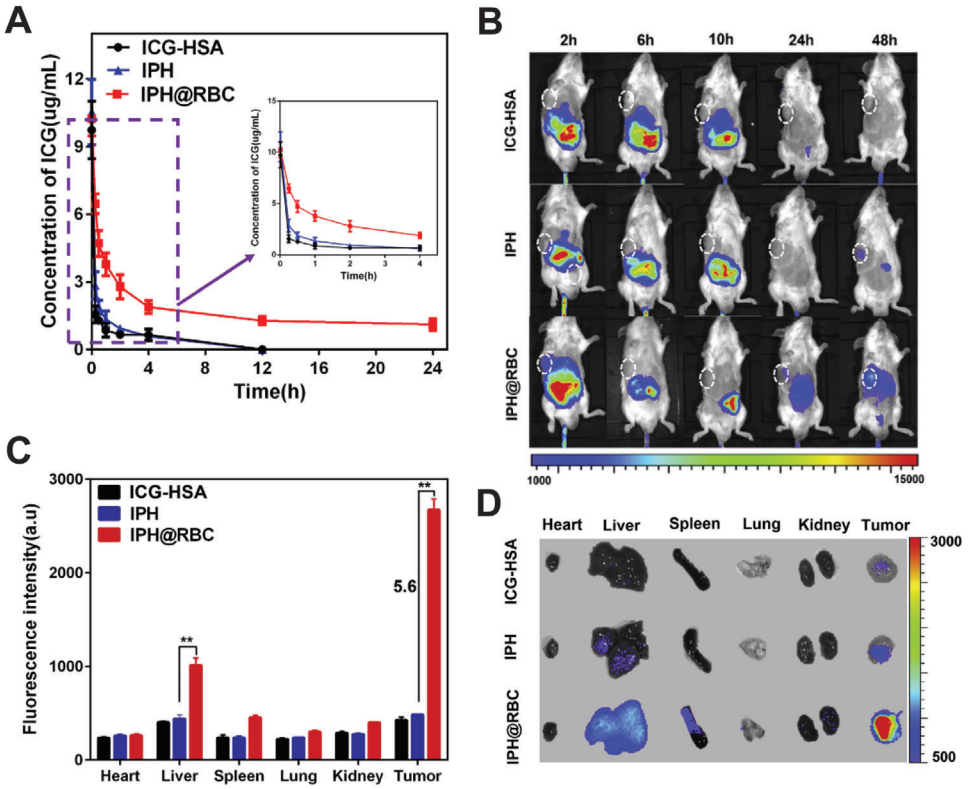

Figure 2. In vivo blood retention and biodistribution of nanoformulations after intravenous injection. A) Blood retentions of ICG-HSA, IPH, and IPH@RBC over 24 h. Data are expressed as the mean ± SEM ($n = 4$). B) Fluorescence images of CT-26 tumor-bearing mice at different time points. C) Nanoformulations biodistribution in mice determined by ICG fluorescence after 48 h of administration. D) Ex vivo NIR fluorescence images of major organs and tumors after 48 h of intravenous injection. The data are shown as mean ± SEM ($n = 3$). Adapted with permission.[127] Copyright 2017, Elsevier.

nanoparticles (i.e., 5.8-fold higher blood retention time). After 24 h of administration, the PTX plasma concentration was 1.4 ± 0.2 μg mL^{-1} for the RBC-coated nanoparticles, which was 9.9-fold higher than that of PTX-loaded polymeric nanoparticles. When combined with iRGD, RBC mimetic nanoparticles presented an inhibition of the tumor growth in 90% and lung metastasis in 95%, whereas PTX-loaded nanoparticles, PTX/iRGD, and RBC mimetic nanoparticles groups only reduced the tumor growth in 46.1%, 64.8%, and 65.6%, respectively. Altogether, the data available in the literature reinforce the importance of prolonging the nanocarrier blood circulation and tumor specificity for developing more efficient anticancer therapies.

4.3. Platelet Cell-Derived Vesicles Camouflage Nanoparticles

Platelets (PLTs) are small non-nucleated cell fragments (≈2–4 μm in diameter) with a lifespan of 5 to 10 days.[164] PLTs are derived from the fragmentation of megakaryocytes and are specialized circulating cells that play a key role in homeostasis and thrombosis.[165,166] PLTs are considered "circulating sentinels" with the main function to target sites with vascular injuries and trigger the repair processes, prevent bleeding, as well as minimize vascular injury. Compared to RBCs, PLTs are more complex and present higher variability of receptors on their surface (e.g., P-Selectin, GPIb-IX-V, GPIa-IIa), which enable their action in multiple physiological processes, including immunity, angiogenesis, inflammation, and vessel remodeling.[164,165,167] Therefore, PLTs-based nanomaterials are multifunctional therapeutics that can be applied in a wide range of medical conditions, such as wound healing, arteriosclerosis, and bacterial infections.[168–170]

The presence of markers of immune evasion (e.g., CD47, CD55, and CD59) on the PLTs' membrane also indicates the potential of the PLT-derived vesicles to originate nanomaterials with prolonged blood circulation times.[136,171,172] Furthermore, the expression of specific proteins such as the P-selectin, which presents a high affinity toward CD44 receptors overexpressed in cancer cells, can be further explored for developing PLT-based nanomaterials targeting cancer cells, both in solid tumors or metastasis.[136,173,174] Some studies have been linking PLTs to tumor metastasis, particularly to circulating tumor cells (CTCs) that are disseminated from the primary tumor tissue to the bloodstream. CTCs overexpress a ligand for P-selectin that promotes the activation and aggregation of PLTs around them. Once shielded by PLTs, CTCs are protected from immune recognition, which prolongs their circulation time and facilitates their spreading in the human body.[174,175] Moreover, the PLTs facilitate the epithelial-to-mesenchymal cellular transition, secret

growth factors that stimulate the proliferation of cancer cells, and can also release angiogenic regulators contributing to tumor angiogenesis and promoting cancer growth.[174]

Based on these PLTs/cancer cells' interactions, nanoparticles' functionalization with PLT-derived vesicles may also originate an enhanced and targeted antitumoral therapy.[104,136,138] Rao et al. coated Fe_3O_4 magnetic nanoparticles with PLT-derived vesicles (PLT-MNs) for application in tumor diagnosis (MRI) and photothermal therapy, using RBC-derived vesicles-coated MNs (RBC-MNs) as control.[104] The authors reported that RBC and PLT-MNs nanoparticles presented a similar uptake by macrophages, which was ≈2 times lower than that observed in noncoated nanoparticles. Moreover, the PLT-MNs showed a ≈7 times higher uptake by MCF-7 tumor cells when compared to RBC-MNs and bare nanoformulations, after 24 h of incubation. Such data were further confirmed in the in vivo studies performed in MCF-7 tumor-bearing mouse models. Both RBC and PLT-based MNs nanoparticles showed similar blood circulation times, over 48 h, and a reduced RES uptake, when compared to bare nanoparticles. Furthermore, after 48 h, the PLT-MNs nanoparticles exhibited significantly higher accumulation in the tumor site (≈1.7 times higher than RBC-MNS), and both PLT-MNs and RBC-MNs had lower accumulation in RES organs (≈1.1 to 1.2 lower) than bare nanoparticles. The authors further assessed the establishment of the ABC phenomenon for PLT-MNs, observing no significant changes in the mice's IgM and IgG levels 30 days after injection, whereas a PEGylated control group showed five times higher IgM and IgG levels. Therefore, after 16 days of treatment, the mice treated with PLT-MNs nanoparticles under NIR irradiation exhibited a dramatic tumor regression over time, with ≈6-fold higher tumor weight loss than RBC-MNs nanoparticles treated mice, in the same treatment conditions. Similarly, Hu et al. developed PLT-derived vesicle-coated nanoparticles loaded with doxorubicin (DOX) and TNF-related apoptosis-inducing ligand (TRAIL-induce tumor cells' apoptosis by binding to death receptors).[136] The TRAIL-DOX-PM-NV nanovehicles had a 5.8 times higher half-life in the blood when compared to noncoated nanoparticles, an increase from 5.6 ± 1.4 to 32.6 ± 2.7 h. In accordance, the PLT nanovehicles (PM-NVs) also presented a lower macrophage uptake, ≈4 times lower than noncoated nanoparticles. The fluorescence intensity of PM-NV nanoparticles at the tumor site was 1.9-fold higher than that of noncoated nanoparticles, also presenting 3.0- and 4.5-fold higher fluorescence in tumors than that observed on the liver and kidneys, respectively. Furthermore, the mice treated with TRAIL-DOX-PM-NV nanoformulation showed a remarkable volume reduction compared to the other formulations (≈2-, ≈3-, and ≈5-fold lower tumor volume than DOX-PM-NV, TRAIL-PM-NV, and TRAIL-DOX-NV, respectively), with an almost complete tumor eradication. Moreover, after the injection of MDA-MB-231 cells in nude mice, the group treated with noncoated nanoparticles developed extended nodules in the lung without significant differences to the saline-treated mice. By contrast, the TRAIL-DOX-PM-NV significantly reduced the establishment of metastatic nodules from ≈60 nodules to ≈10 nodules, which can be attributed to the CTCs' elimination from the bloodstream due to the PLT-derived vesicles' P-selectin targeting. With the same purpose, Jing et al. designed a novel nanomedicine by encapsulating melanin nanoparticles (MNPs) and DOX on an RGD peptide-modified nanoscale platelet vesicle (RGD-NPVs@MNPs/DOX) for tumor and metastases treatment (**Figure 3**).[107] The preliminary pharmacokinetic studies revealed that the PLT vesicle coating increased five times the blood half-life of the nanoparticles, from 5.13 ± 2.61 to 27.6 ± 4.1 h (NPVs@MNPs/DOX) and 26.4 ± 3.2 h (RGD-NPVs@MNPs/DOX). Moreover, the PLT vesicle coating also reduced the nanoparticles' accumulation in RES major organs, which was in accordance with the 67.5% reduction in the uptake by macrophages when compared to the lipidic formulation (NLVs@MNPs/DOX), after 4 h of incubation. Such was also followed by a gradual RGD-NPVs@MNPs/DOX accumulation in the tumor tissue during the 24 h postinjection (≈4.6 times higher than the fluorescence observed after 2 h). Moreover, the NPVs@MNPs/DOX treated mice showed an increase in the tumor volume to ≈173 mm^3, whereas in the RGD-NPVs@MNPs/DOX group the tumor volume decreased to ≈20 mm^3, after the photothermal and chemotherapeutic treatment. Simultaneously, the authors observed that this dual-treatment mediated by RGD-NPVs@MNPs/DOX was able to completely inhibit the development of lung tumor metastasis, whereas the other groups showed metastatic nodules (with ≈8, 7, 6, 3, and 2 lung nodules observed in PBS, DOX, NPVs@MNPs/DOX, RGD-NPVs@MNPs/DOX, and NPVs@MNPs/DOX + laser mice treated group, respectively).

Thus, PLT-mimicking nanosystems present some advantages over RBC-derived vesicles coated nanocarriers, namely, their inherent targeting capacity. Although promising, when compared to RBCs, PLTs present a lower availability for extraction and a shorter lifetime, which makes challenging a large-scale application.[167,176]

4.4. Cancer Cell-Derived Vesicles Camouflage Nanoparticles

As discussed above, the RBC-derived vesicles show a prolonged circulation time, reduced macrophage uptake, and low immune system recognition. However, the RBC-derived vesicles lack the intrinsic capacity to actively target the tumor tissues. Similar to PLTs, cancer cell-derived vesicles present the capacity to specifically target primary tumors and metastatic sites.[177] These cancer cell-derived vesicles can take advantage of surface adhesion molecules (e.g., N-cadherin, galectin-3, epithelial cell adhesion molecules) that in the cancer cells are responsible for their binding and aggregation. Therefore, this approach can combine the tumor specificity with the cancer cells' innate capacity to evade the immune system, leading to nanomaterials with enhanced pharmacokinetics.[177–180] For example, the coating of ICG-loaded poly(lactic-*co*-glycolic acid) (PLGA) nanoparticles with MCF-7 derived vesicles (ICNPs) resulted in a cell-type specific uptake, two times higher in MCF-7 cells than in A549 or MDA-MB-231 cell lines.[113] Moreover, the ICNPs presented 7–14 times higher blood concentration than the free ICG administration, 1 h after administration. The AUC (the area under the plasma drug concentration–time curve for 24 h) of ICNPs was also superior to that of the free ICG, 24 h after administration, increasing from 35 to 411 μg min^{-1} mL^{-1}. Accordingly, the ICNPs showed a reduced RES organs uptake, as well as 3.1- and 4.75-fold increased tumor accumulation when compared with bare nanoparticles and free ICG, respectively (**Figure 4**).

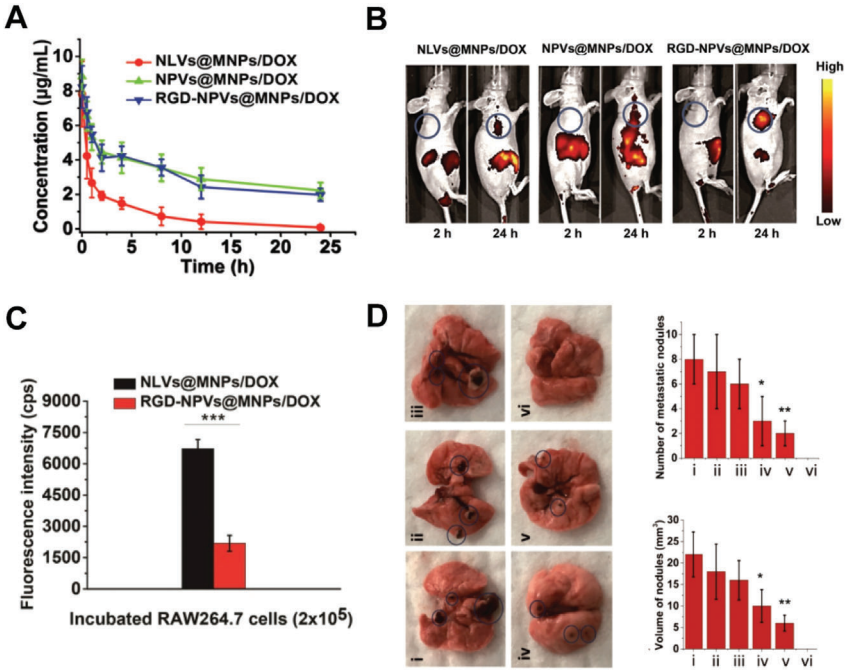

Figure 3. In vivo blood retention, biodistribution, and anti-metastases effect of nanoformulations after intravenous injection. A) Blood circulation time of NLVs@MNPs/DOX, NPVs@MNPs/DOX, and RGD-NPVs@MNPs/DOX in mice bearing MDA-MB-231/ADR tumors during 24 h. B) Fluorescence images of mice bearing tumors at 2 and 24 h after nanoformulations intravenous administration. C) Fluorescence intensities of RAW264.7 cells after incubation with RGD-NPVs@MNPs/DOX and NLVs@MNPs/DOX for 4 h. D) Representative images of the lung with respective number and volume of metastatic at 22 days after the treatments. i) PBS; ii) DOX; iii) NPVs@MNPs/DOX; iv) RGD-NPVs@MNPs/DOX; v) NPVs@MNPs/DOX + laser; vi) RGD-NPVs@MNPs/DOX + laser. $*p < 0.05$; $**p < 0.01$; $***p < 0.001$. Adapted with permission.[107] Copyright 2018, Ivyspring.

Similarly, Shao et al. developed an X-ray-responsive diselenide bridged-4T1 breast cancer cell-derived vesicles coated mesoporous organosilica (CM@MON@DOX) nanoparticle for the delivery of DOX and the PD-L1 immune checkpoint for the cancer chemo-immunotherapy.[116] The in vitro studies revealed that the CM@MON@DOX nanoparticles presented higher internalization in 4T1 cells and simultaneously reduced the uptake by RAW264.7 macrophages. Furthermore, the biodistribution assays showed that the 4T1-derived vesicles resulted in a ≈3 times higher blood half-life when compared to bare nanoparticles, i.e., 18.4 and 6.6 h, respectively. Such, further rendered to the CM@MON@DOX nanoparticles the highest tumor accumulation and lowered the uptake by RES organs, 12 h postinjection. In another work, Nie et al. coated the PEGylated liposomes containing mesoporous silica cores with MCF-7-derived vesicles (CCM@LM).[181] The nanomaterials' incubation with different cell lines (MCF-7, Huh-7, Caco-2, and HeLa) for 2 h showed a superior internalization on the homologous MCF-7 cells (≈80%) followed by Huh-7 cells (≈50%). Moreover, the CCM@LM also presented a reduced protein adsorption with no significant changes in their size or charge, whereas the noncoated counterparts (LM) showed a zeta potential variation of ≈25 mV. Accordingly, the LM nanoparticles showed a 4.9-fold higher fluorescence intensity fluorescence in J774A.1 macrophages cells, when compared to CCM@LM nanoparticles. The biodistribution studies revealed that after 24 h, the CCM@LM presented a 5.3-fold higher accumulation at the tumor site than LM nanoparticles. Additionally, CCM@LM nanoparticles displayed the highest penetration capacity into multicellular spheroids at all scanning depths. Such data justify the highest tumor growth reduction (i.e., 95% tumor inhibition) observed in the mice treated with CCM@LM nanoparticles.

Despite the cancer cell-derived vesicles being less effective than RBC ones in enhancing the blood circulation time, this strategy shows a higher tumor-specific targeting capability. Moreover, their application can be combined with immunological adjuvants to also stimulate the activation of the immune system and improve the nanoparticles' anticancer efficacy.[116,182] However, the risk of autoimmunity (tumor cells express some antigens also found in healthy cells) is still present and the purification process often leads to variability in the antigens present at the vesicles' surface.[177,183]

4.5. Immune Cells-Derived Vesicles Camouflage Nanoparticles

Leukocytes, also known as white blood cells, present a life span from a few days to months and are permanently released into circulation. Leukocytes can be divided into two mains classes: granulocytes, which include eosinophil, basophil, and neutrophil; and agranulocytes which include lymphocytes (T and B lymphocytes and NK cells) and monocytes (that can be differentiated into dendritic cells and macrophages). After maturation, the leukocytes enter the blood circulation and can migrate to extravascular inflammatory and infection sites. In fact, to guarantee an immediate and efficient response to the invasion, numerous

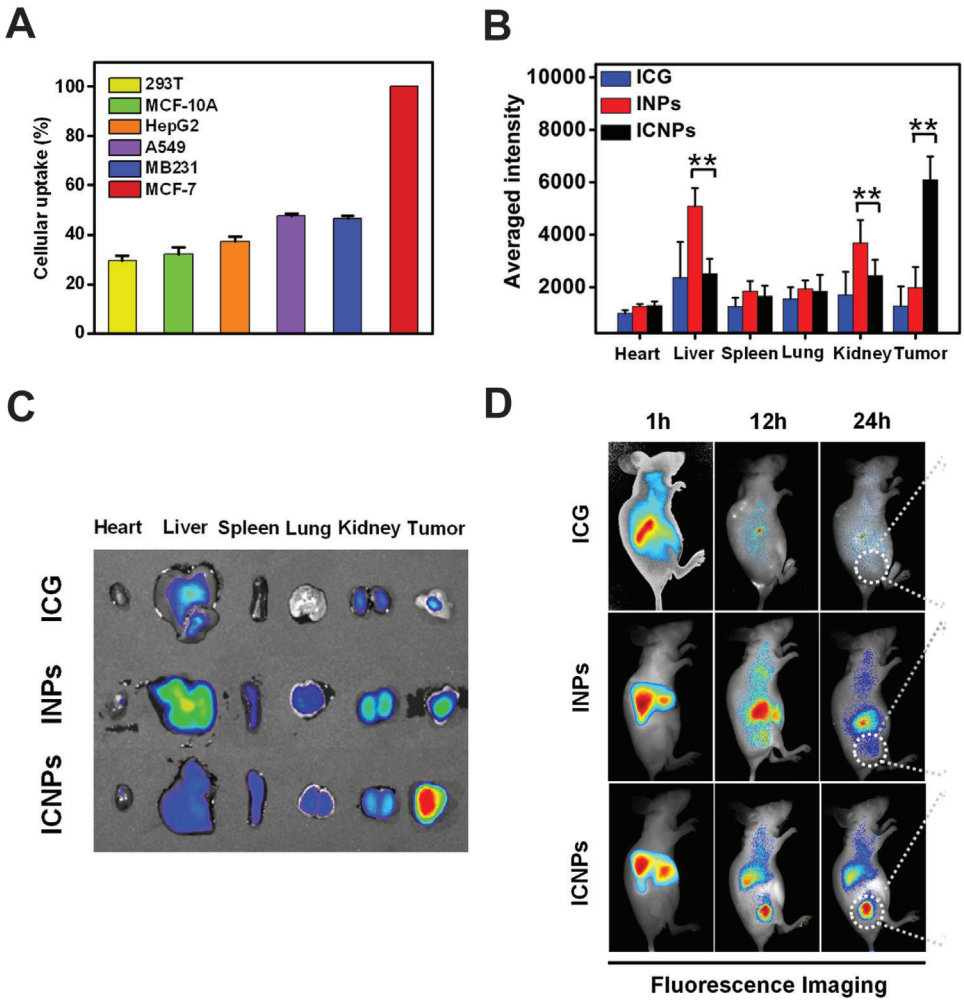

Figure 4. In vitro cellular uptake and in vivo biodistribution of nanoformulations after intravenous injection. A) Cellular uptake of six cell lines, 293T, MCF-10A, HepG2, A549, MB231, and MCF-7 cells, upon 2 h of incubation with ICNPs. B) Biodistribution of free ICG, INP, and ICNPs in nude mice, determined by the average fluorescence intensity of each organ after 12 h. C) Ex vivo NIR images of the tumor and major organs after 24 h of administration with free ICG, INPs, and ICNPs. D) In vivo images of nude mice, where ICNPs exhibited a homologous-targeting effect. The data are shown as mean ± SD ($n = 3$); $*p < 0.05$, $**p < 0.01$. Adapted with permission.[113] Copyright 2016, American Chemical Society.

leukocytes are present in the bloodstream as well as in the secondary lymphoid tissues, allowing a fast release to the inflammatory sites.[102,184,185] Currently, it is recognized that chronic endothelial inflammation is a characteristic of tumors, where different immune cells can play a critical role in cancer establishment, development, and progression.[184,186] Among leukocyte cells, macrophages are the main immune cells present in the tumor microenvironment—also denominated as tumor-associated macrophages (TAMs). TAMs surround tumor cells and interact with each other contributing to tumor growth, progression, and metastasis. Thus, TAMs membrane can be an excellent tool to camouflage nanoparticles with the potential for increasing blood circulation time and tumor targeting. The expression of surface proteins on macrophages' cell membrane, such as Toll-like receptors and interleukin-1 receptors, is one of the main reasons for the active tumor targeting ability.[187–189] Also, the expression of CD49d (α4 integrin) surface marker, a ligand to adhesion molecule 1 (VCAM) expressed by cancer cells, further enables the macrophages binding to cancer cells. Thus, such affinity toward cancer cells can also prompt the elimination of metastatic cancer cells.[187,188] Furthermore, tumor cells secret the immunoregulatory molecule CSF1, which activates a signaling pathway that is responsive to the TAMs immunosuppressor phenotype. Therefore, the blockage of CSF1 interaction with the receptor on the TAMs surface can prevent the immunosuppressor action of cancer cells. Thus, nanoparticles coated with TAMs-derived vesicles can induce a competitive inhibition between the tumor cells and the TAMs, which may bypass the cancer cells' immunosuppression.[102,187,190–192] Xuan et al. reported that the coating of Au nanoshells with macrophage cell-derived vesicles (MPCM-AuNSs) enhanced the blood retention time.[143] In fact, the bare nanoparticles were almost eliminated from the blood, 24 h after administration, whereas more than 30% of MPCM-AuNSs were still detected in blood vessels after 48 h. Moreover, macrophage-coated nanoparticles presented a remarkably increased tumor accumulation and lower uptake

by RES organs, compared with bare nanoparticles. The MPCM-AuNSs treated group presented 7.48% ID g^{-1} accumulated in the tumor tissue 48 h after administration, contrasting with the 1.61% ID g^{-1} of noncoated nanoparticles. With a similar strategy, Li et al. developed a DNA tetrahedron dendrimer that was sequentially coated with a liposome and a macrophage-derived vesicle (DOX-MPK@MDL) for the treatment of lung metastases of breast cancer.[118] Confocal microscopy studies revealed that DOX-MPK@MDL presented higher internalization into 4T1 cells than bare nanoparticles, being the DOX mainly accumulated in the cells' nucleus 4 h after administration. Moreover, after the establishment of 4T1-luc tumors and lung metastasis in BABL/c nude mice, the DOX-MPK@MDL group presented 2.1-fold higher fluorescence intensity in the lungs than bare nanoparticles, inducing a 78% inhibition in the lung metastases when compared to bare nanoparticles.

Besides macrophages, other leukocytes can be explored as sources for the extraction of cell-derived vesicles. Neutrophils are the most abundant leukocytes in humans and correspond to the main cells recruited during inflammation (e.g., tumors) and to infection sites.[193,194] Their membrane presents receptors highly sensitive to the inflammatory cytokines, which make the neutrophil-derived vesicles innately targeted toward the tumors.[195,196] For example, Kang et al. developed carfilzomib (CFZ) loaded PLGA nanoparticles with neutrophil-derived vesicles (NM-NPs) to target metastases in 4T1 mouse models.[122] The blood circulation half-life of bare nanoparticles, PEGylated-PLGA-NPs, and NM-NPs was 0.77, 4.73, and 6.59 h, respectively. Additionally, the AUCs of PEGylated-PLGA-NPs and NM-NPs were 134.4- and 207.2-fold higher than that of bare nanoparticles. Moreover, the NM-NPs showed an accumulation in lung metastatic foci 2.12- and 3.02-fold higher than that of bare nanoparticles and PEGylated-PLGA-NPs, respectively. Therefore, the mice treatment with NM-NPs-CFZ led to an obvious tumor inhibitory effect with an 87.2% reduction of the metastasis foci at the end of the treatment.

Similarly, natural killer (NK) cells are the first line of defense in innate immunity and have also been explored to camouflage nanoparticles.[197] NK cells can regulate the immune response through the secretion of cytokines, stimuli of antigen-presenting cells maturation, and induction of proinflammatory M1-macrophages polarization (macrophages with antitumoral function, able to distinguish normal cells from cancer cells). NK cells distinguish malignant cells from normal cells via surface inhibitory receptors (e.g., NKG2D, NKp44) and can stimulate tumor cells' apoptosis via surface death ligands/receptors interaction (e.g., FAS ligand and TRAIL).[146,197,198] Thus, this ligand–receptor interaction can also be explored by the nanomaterials to potentiate the anticancer effectiveness.[146,199,200] In fact, an NK cell line (NK-92 cells) isolated in 1992 from a man with malignant non-Hodgkin's lymphoma, presented strong antitumor effects in a variety of cancer cells without prior sensitization. NK-92 has undergone preclinical development and completed phase I trials in cancer patients (NCT00900809 and NCT00990717). Importantly, NK-92 cells—in contrast to blood NK cells—can be easily modified to express specific ligands to target cancer cells.[201,202] Deng et al. developed NK-derived vesicles containing PLGA nanoparticles loaded with the photosensitizer TCPP for the treatment of primary and distant tumors.[146] Flow cytometry studies revealed that NK-NPs/TCPP fluorescence intensity on cancer cells was five times higher than that obtained with bare nanoparticles (T-NPs) and 32 times stronger than in normal cells. Mice studies showed that NK-NPs accumulated in the tumor tissue during the first 24 h and then gradually decrease with time, showing a six times higher accumulation in 4T1 tumors than T-NPs. Furthermore, the NK-NPs presented a blood half-life of 8 h, whereas in T-NPS this value was 5.5 h. Moreover, when compared to the control and T-NPs group, the NK-NPs significantly increased the expression of M1 macrophages markers, i.e., iNOS/CD86, and cytokines (TNF-α, IL-6, and IL-12), while simultaneously decreased the expression of the M2 macrophages marker, i.e., CD206. Also, NK-NPs significantly enhanced the dendritic cells (DCs) maturation, being 3 and 2.5 times higher than that observed in PBS and T-NPs treated mice.

DCs are the most potent antigen-presenting cells, playing a pivotal role in the activation of both innate and adaptative immune responses. DCs can be key participants in cancer immunotherapy presenting a strong ability to activate antigen-specific T cells, which consequently can be differentiated into helper, cytotoxic, or regulatory cells.[203–205] As a matter of fact, a DC-based vaccine has already been approved by FDA for prostate cancer treatment.[206] In this way, apart from the enhancement of the pharmacokinetic profile, the development of nanomaterials coated with DC-derived can be explored to deliver immune regulators specifically to T cells, potentiating the antitumoral immune response.[207,208] Finally, the vesicles originating from T cells can maintain the T cell receptors (TCRs) that are capable of specifically detecting and binding to tumor-derived antigens, and consequently, create a promising tumor-targeted nanomaterial.[147,209–211] For example, Han et al. developed azide (N_3)-modified T cell-derived vesicle containing ICG-loaded PLGA nanoparticles (N_3-TINPs) with tumor targeting and immune recognition properties.[147] The pharmacokinetics studies revealed that the of N_3-TINPs treated group presented a higher ICG concentration in the blood than INPs nanoparticles, 15 min postinjection. The AUC_{24h} of N_3-TINPs (360 μg min mL^{-1}) was fourfold higher than that detected of INPs (84 μg min mL^{-1}). In vitro studies show that Raji cancer cells treated with N_3-TINPs had a higher ICG fluorescence than that observed in cells treated with TINPs (≈1.3 times higher), INPS (≈2.2 times higher), and free ICG (≈3.5 times higher). Furthermore, the blocking of TCR on nanoparticles (incubation with anti-TCR antibody), inhibited the recognition of Raji cells by TINPs and N_3-TINPs, with a 40% and 30% decrease in ICG fluorescence, respectively, which confirmed that the immune recognition of T cell membrane-specific receptors is crucial for targeting the tumor cells. After 48 h, the mice treated with INPs exhibited a weak fluorescence signal in the tumor, whereas T cell-coated nanoparticles (TINPs and N_3-TINPs) groups showed increased ICG fluorescence. Particularly, the N_3-TINPs treated group presented ≈30% and ≈50% higher fluorescence intensity in tumors than that obtained in mice treated with TINPs and INPs, respectively (**Figure 5**).

Despite the promising results obtained using leukocyte-derived vesicles, the expression of major histocompatibility complex molecules on the obtained immune membranes can lead to an inflammatory response, which can be ameliorated if the patient's immune cells are used to design the nanomaterial.[102,212]

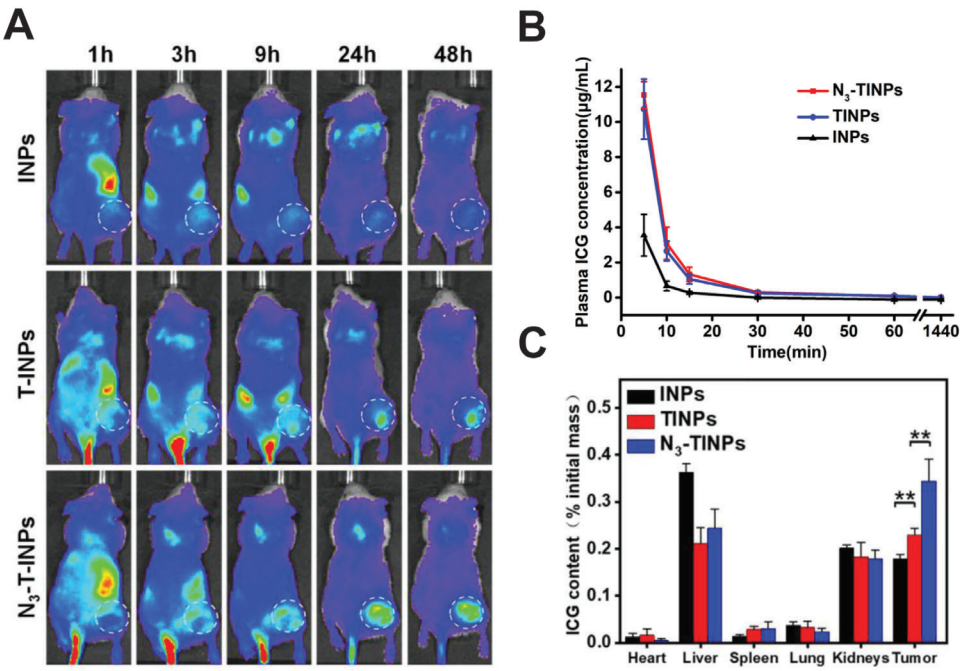

Figure 5. Nanoformulations in vivo biodistribution and blood retention after intravenous administration. A) In vivo imaging of mice at different time points after nanoformulations injection. B) Pharmacokinetic profile of nanoparticles based on blood ICG concentration. C) The ICG content of each organ was quantified to analyze the nanoparticles' biodistribution. Statistical *p*-values: $^{**}p < 0.01$. Adapted with permission under the terms of the CC-BY license.[147] Copyright 2019, the authors. Published by Wiley-VCH GmbH.

4.6. Hybrid Cell-Derived Vesicles Camouflage Nanoparticles

Hybrid or heterogenous cell-derived vesicles can be developed by combining membranes isolated from two or more cell types or even other synthetic lipids. Such is commonly achieved through the simultaneous coextrusion of different materials.[106] Therefore, the hybrid cell-derived vesicles will present a structure comprising the different constituents of the original cells. In this way, the nanomaterials can be engineered to combine the RBCs' prolonged blood circulation time and immune evasion (CD47 "don't eat me" signalization) with the increased tumor specificity observed with PLTs, leukocytes, and homologous cancer cells (**Figure 6**).[151,213–215]

Wang et al. developed a hybrid membrane camouflaged nanoparticles to functionalize DOX-loaded hollow copper sulfide nanoparticles.[149] The hybrid membrane (CuS@[RBC–B16]) resulted from the fusion of RBC and melanoma cells (B16-F10 cells)-derived vesicles. The in vitro studies showed that hybrid nanoparticles have 8.25 and 9.78 times higher internalization in B16-F10 cancer cells than in HT1080 or NHDF cells, respectively. Such demonstrates that the heterogenous structure retains the B16-F10-derived vesicles' self-targeting capacity. Moreover, the biodistribution data revealed that the blood retention of hybrid (CuS@[RBC–B16]) nanomaterials, 20.2% ID g^{-1}, was slightly lower than that of RBC coated (CuS@RBC; 22.9% ID g^{-1}) and higher than that of B16-F10-coated (CuS@B16; 14.5% ID g^{-1}) and bare (CuS; 5.2% ID g^{-1}) nanoparticles (**Figure 7**). Accordingly, the blood circulation half-life of CuS@[RBC–B16] and CuS@RBC nanoparticles was 9.6 and 9.9 h, whereas this value decreased to 6.0 h for CuS@B16 and 1.0 h for bare nanoparticles. More importantly, the hybrid nanoparticles presented 1.5-, 1.4-, and 2.5-fold higher tumor accumulation than CuS@RBC, CuS@B16, and bare nanoparticles, respectively. In turn, hybrid nanoparticles' accumulation in the spleen and liver was reduced by 34.6% and 23% when compared with bare nanoparticles.

Liu and co-workers developed RBC–PLT membrane-coated polypyrrole (PPy) nanoparticles for mediating a cancer photothermal treatment.[156] The hybrid coating led to increased blood retention, 11.5% and 8.9% ID g^{-1} at 24 and 48 h after injection, contrasting with the 3.1% and 1.7% ID g^{-1} of single-coated platelets nanoparticles. Moreover, the treatment mediated by hybrid nanoparticles resulted in higher tumor inhibition, an average tumor weight of 0.136 g, whereas the mice treated with single-coated PLT or RBC nanoformulations presented tumors with 0.346 and 0.420 g, respectively. Such difference in the antitumoral efficacy is an indicator of the PLTs-mediated tumor targeting. In another work, DOX-loaded PLGA nanoparticles were coated with a hybrid-membrane derived from macrophages RAW264.7(RAW) and 4T1 cells for the treatment of lung metastases of breast cancer.[151] In vitro studies demonstrated the homologous targeting capacity of DPLGA@[RAW-4T1] nanoparticles, with a two- to fourfold higher fluorescence intensity in 4T1 cells than in other cell groups. Moreover, the DPLGA@[RAW-4T1] hybrid nanoparticles also presented higher internalization in 4T1 cells (88.70%) than the single-coated counterparts DPLGA@RAW (72.30%) and DPLGA@4T1 (74.23%). In turn, the hybrid nanoparticles exhibited an excellent chemotherapeutic potential reducing by 88.9% the breast cancer-derived lung metastases, whereas this value was lower, i.e., 80.6% and 77.8%,

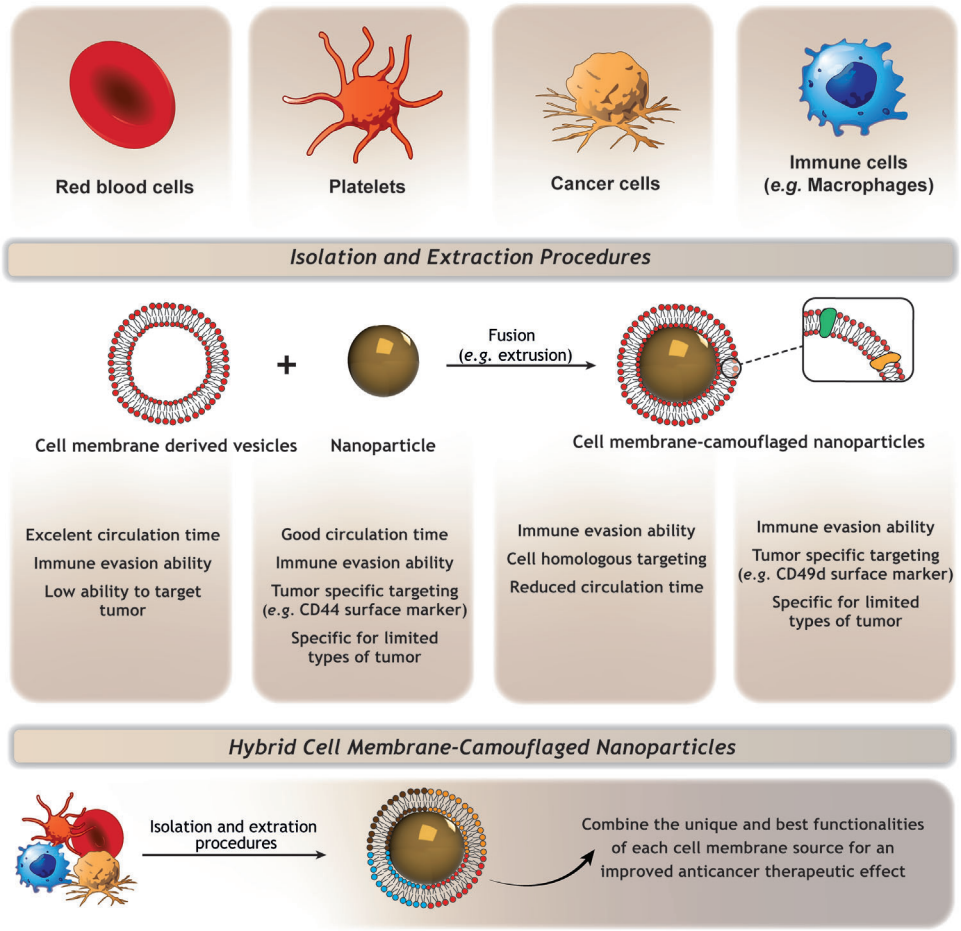

Figure 6. Representation of the main cell sources explored to camouflage nanoparticles and their contribution to improving the nanoparticles' therapeutic effect.

for the DPLGA@4T1 and DPLGA@RAW treated mice, respectively.

5. Challenges and Outlooks

Despite the broad range of applications of biomimetic membranes, there are still some challenges that must be overcome before their effective translation to the clinic. First, the process of membrane extraction and fusion with nanoparticles can be complex and difficult to control, which introduces several variables and reproducibility issues (e.g., single or multiple cell sources, isolation/extrusion techniques, single or multilamellar vesicles, and composition of cell-derived vesicles).[21,102,106] Furthermore, the isolated cell membrane fragments and cell-derived vesicles need to be stored under specific conditions (e.g., cold temperature and enzymes-free environment), to guarantee the stability of the lipids, proteins, and carbohydrates.[105,112] Additionally, the scale-up of the production process is challenging, since it should be carried out aseptically and there is the necessity for a high number of cells.[114] RBCs and PLTs are present in high quantities in the blood which favors their isolation and application. However, for other cell types (e.g., cancer and immune cells) their isolation and manipulation can be more difficult. Moreover, in hybrid cell-derived vesicles, the determination of the fraction of each cell source is laborious and the batch-to-batch reproducibility is still far from ideal. Therefore, it is crucial to develop, optimize, and standardize the extraction procedures/technologies to maximize yield, purity, homogeneity, and long-term storage. Furthermore, the data available in the literature have been showing that the coating of the nanoparticles with cell-derived vesicles also decreases the accumulation in major organs. However, the long-term interaction of these nanoparticles with metabolic organs (e.g., liver and spleen) should not be ignored and further research is still necessary.

Despite these challenges, nanoparticles' biomimetic shells in association with a wide variety of core types (e.g., polymers, metals, drugs) provide a unique strategy for developing novel and more effective anticancer therapeutics. Moreover, the application of patients' cells to create the nanoparticles coated with cell-derived vesicles can be explored to avoid possible immunological issues, improve the nanomaterials' tumor accumulation, and enhance the antitumoral efficacy.[216,217] Additionally, the utilization of smart nanomaterials (i.e., stimuli-responsive materials) as cores will allow the development of spatiotemporally controlled therapies largely reducing off-target cytotoxicity and increasing the therapeutic effectiveness.[218,219]

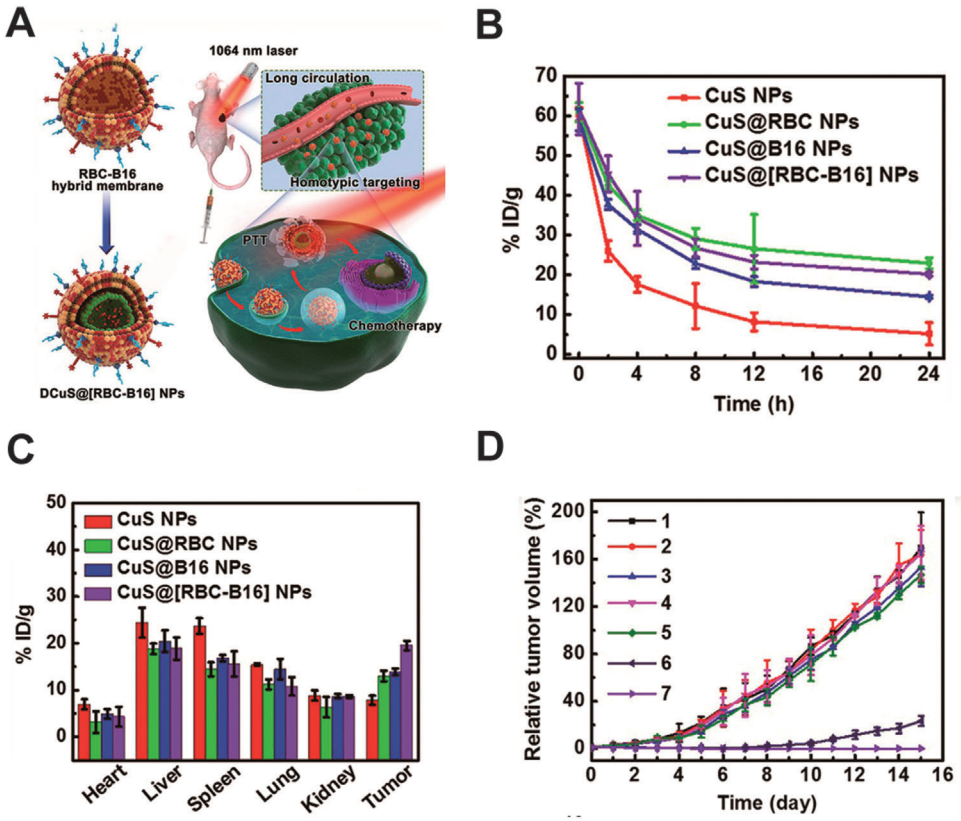

Figure 7. In vivo blood retention, biodistribution, and tumor volume inhibition after nanoformulations' intravenous administration. A) Schematic of hybrid membrane camouflaged DOX-loaded hollow copper sulfide nanoparticles DCuS@[RBC-B16]. B) Blood retention and C) biodistribution of CuS@NPs, CuS@RBC NPs, CuS@B16 NPs, and CuS@[RBC-B16] NPs, 24 h after administration. D) Analysis of the relative tumor volume variation on melanoma-bearing mice (1: NS, 2: CuS@[RBC-B16], 3: DOX, 4: NIR laser (1064 nm, 1 W cm^{-2}), 5: DCuS@[RBC-B16], 6: CuS@[RBC-B16] with NIR laser (1064 nm, 1 W cm^{-2}), 7: DCuS@[RBC-B16] with NIR laser (1064 nm, 1 W cm^{-2}). Adapted with permission.[149] Copyright 2018, American Chemical Society.

6. Conclusion

Until now the application of nanoparticles in cancer therapy has been showing promising results, improving the efficacy and security of the therapeutics payloads. Despite this, only a reduced number of nanomedicines were approved for clinical use. In fact, less than 1% of the administered nanoparticles' dose effectively reaches the tumor, which means that nanoparticles are prematurely eliminated from the body or accumulate in off-target tissues. Once administrated, nanoparticles are almost instantly coated with blood proteins, forming a protein corona, a phenomenon that is considered a determinant factor in the pharmacokinetic profile and therapeutic performance of nanoparticles. Therefore, limiting the interactions of nanoparticles with blood components could lead to a prolonged blood circulation time that consequently improves the chances of nanoparticles being retained in the tumor and exerting their therapeutic effect. With this in mind, several strategies have been developed to improve nanoparticles' circulation time, mainly by their surface modification with hydrophilic polymers or biomimetic coatings. The nanoparticles' coating with cell-derived vesicles emerged in recent years as a powerful strategy in cancer treatment. The cell-derived vesicles retain the antigenic diversity of the source cell, providing immune escape, targeting ability, and cellular-related functions. RBC-derived coatings were the first ones explored to functionalize and improve nanomaterials' pharmacokinetic profile and therapeutic effect. Currently, this approach was extended to other cell types which made it possible to expand this biomimetic nanotechnology for the diagnosis and treatment of several diseases. In general, the RBC-derived vesicles show a higher capacity to increase the nanoparticles' blood circulation time, whereas the cell-derived coatings formed from PTLs, immune, and cancer cells often show higher bioactivity (e.g., tumor targeting). Therefore, the application of hybrid cell-derived vesicles to coat nanoparticles presents advantages over the simpler single-cell-derived vesicles, making them exciting platforms for developing nanomedicines with higher antitumoral efficacy, which will accelerate their translation to the clinic.

Acknowledgements

This work was financed by the Foundation for Science and Technology (FCT), through funds from the State Budget, and by the European Regional Development Fund (ERDF), under the Portugal 2020 Program, through the Regional Operational Program of the Center (Centro2020), through the Project with the reference UIDB/00709/2020. The funding from CENTRO-01-0145-FEDER-028989 and POCI-01-0145-FEDER-031462 are also acknowledged. C.F.R. acknowledges for her Ph.D. fellowship from FCT (SFRH/BD/144680/2019). D.d.M.-D. acknowledges

FCT for the financial support given through a Junior Researcher contract (2021.00590.CEECIND). N.F. acknowledges the individual fellowship from UBI-Banco Santander/Totta. The funders had no role in the decision to publish or in the preparation of the manuscript.

Conflict of Interest

The authors declare no conflict of interest.

Keywords

blood circulation, cancer, cell-derived vesicles, nanoparticles, protein corona, stealthing

Received: May 23, 2022
Revised: September 11, 2022
Published online: October 17, 2022

[1] B. Al-Lazikani, U. Banerji, P. Workman, *Nat. Biotechnol.* **2012**, *30*, 679.
[2] B. Shrestha, L. Tang, G. Romero, *Adv. Ther.* **2019**, *2*, 1900076.
[3] M. J. Mitchell, M. M. Billingsley, R. M. Haley, M. E. Wechsler, N. A. Peppas, R. Langer, *Nat. Rev. Drug Discovery* **2021**, *20*, 101.
[4] A. C. Anselmo, S. Mitragotri, *Bioeng. Transl. Med.* **2019**, *4*, 10143.
[5] Y. Yao, Y. Zhou, L. Liu, Y. Xu, Q. Chen, Y. Wang, S. Wu, Y. Deng, J. Zhang, A. Shao, *Front. Mol. Biosci.* **2020**, *7*, 193.
[6] V. Balasubramanian, Z. Liu, J. Hirvonen, H. L. A. Santos, *Adv. Healthcare Mater.* **2018**, *7*, 1700432.
[7] S. Wilhelm, A. J. Tavares, Q. Dai, S. Ohta, J. Audet, H. F. Dvorak, W. C. W. Chan, *Nat. Rev. Mater.* **2016**, *1*, 16014.
[8] M. J. Ernsting, M. Murakami, A. Roy, S.-D. Li, *J. Controlled Release* **2013**, *172*, 782.
[9] A. Rodallec, S. Benzekry, B. Lacarelle, J. Ciccolini, R. Fanciullino, *Crit. Rev. Oncol./Hematol.* **2018**, *129*, 1.
[10] S. Hua, M. B. C. De Matos, J. M. Metselaar, G. Storm, *Front. Pharmacol.* **2018**, *9*, 790.
[11] B. Wang, X. He, Z. Zhang, Y. Zhao, W. Feng, *Acc. Chem. Res.* **2013**, *46*, 761.
[12] X. Duan, Y. Li, *Small* **2013**, *9*, 1521.
[13] S.-Q. Zhang, Q. Fu, Y.-J. Zhang, J.-X. Pan, L. Zhang, Z.-R. Zhang, Z.-M. Liu, *Acta Pharmacol. Sin.* **2021**, *42*, 1040.
[14] H. Nehoff, N. N. Parayath, L. Domanovitch, S. Taurin, K. Greish, *Int. J. Nanomed.* **2014**, *9*, 2539.
[15] Y. Matsumoto, J. W. Nichols, K. Toh, T. Nomoto, H. Cabral, Y. Miura, R. J. Christie, N. Yamada, T. Ogura, M. R. Kano, Y. Matsumura, N. Nishiyama, T. Yamasoba, Y. H. Bae, K. Kataoka, *Nat. Nanotechnol.* **2016**, *11*, 533.
[16] N. Singh, C. L. Marets, J. Boudon, N. Millot, L. Saviot, L. Maurizi, *Nanoscale Adv.* **2021**, *3*, 1209.
[17] R. Rampado, S. Crotti, P. Caliceti, S. Pucciarelli, M. Agostini, *Front. Bioeng. Biotechnol.* **2020**, *8*, 166.
[18] T. T. Hoang Thi, E. H. Pilkington, D. H. Nguyen, J. S. Lee, K.i D. Park, N. P. Truong, *Polymers* **2020**, *12*, 298.
[19] O. Sedlacek, R. Hoogenboom, *Adv. Ther.* **2020**, *3*, 1900168.
[20] R. J. Bose, R. Paulmurugan, J. Moon, S.-H. Lee, H. Park, *Drug Discovery Today* **2018**, *23*, 891.
[21] X. Zhen, P. Cheng, K. Pu, *Small* **2019**, *15*, 1804105.
[22] B. Li, F. Wang, L. Gui, Q. He, Y. Yao, H. Chen, *Nanomedicine* **2018**, *13*, 2099.
[23] D. Chenthamara, S. Subramaniam, S. G. Ramakrishnan, S. Krishnaswamy, M. M. Essa, F.-H. Lin, M. W. Qoronfleh, *Biomater. Res.* **2019**, *23*, 20.
[24] Q. Sun, Z. Zhou, N. Qiu, Y. Shen, *Adv. Mater.* **2017**, *29*, 1606628.
[25] A. E. Nel, L. Mädler, D. Velegol, T. Xia, E. M. V. Hoek, P. Somasundaran, F. Klaessig, V. Castranova, M. Thompson, *Nat. Mater.* **2009**, *8*, 543.
[26] C. F. Rodrigues, C. G. Alves, R. Lima-Sousa, A. F. Moreira, D. de Melo-Diogo, I. J. Correia, in *Advances and Avenues in the Development of Novel Carriers for Bioactives and Biological Agents*, Elsevier, Amsterdam **2020**. p. 283.
[27] J. Fang, W. Islam, H. Maeda, *Adv. Drug Delivery Rev.* **2020**, *157*, 142.
[28] M. A. Subhan, S. S. K. Yalamarty, N. Filipczak, F. Parveen, V. P. Torchilin, *J. Pers. Med.* **2021**, *11*, 571.
[29] M. Sharifi, W. C. Cho, A. Ansariesfahani, R. Tarharoudi, H. Malekisarvar, S. Sari, S. H. Bloukh, Z. Edis, M. Amin, J. P. Gleghorn, T. L. M. T. Hagen, M. Falahati, *Cancers* **2022**, *14*, 2868.
[30] R. Ngoune, A. Peters, D. Von Elverfeldt, K. Winkler, G. Pütz, *J. Controlled Release* **2016**, *238*, 58.
[31] A. S. Drozdov, P. I. Nikitin, J. M. Rozenberg, *Int. J. Mol. Sci.* **2021**, *22*, 13011.
[32] J. Park, Y. Choi, H. Chang, W. Um, J. H. Ryu, I. C. Kwon, *Theranostics* **2019**, *9*, 8073.
[33] M. R. Junttila, F. J. De Sauvage, *Nature* **2013**, *501*, 346.
[34] Y. R. Zhang, R. Lin, H. J. Li, H.e Wl, J. Z. Du, J. Wang, *Wiley Interdiscip. Rev.: Nanomed. Nanobiotechnol.* **2019**, *11*, 1519.
[35] P. Foroozandeh, A. A. Aziz, *Nanoscale Res. Lett.* **2018**, *13*, 1.
[36] C. Holohan, S. Van Schaeybroeck, D. B. Longley, P. G. Johnston, *Nat. Rev. Cancer* **2013**, *13*, 714.
[37] M. Zhang, S. Gao, D. Yang, Y. Fang, X. Lin, X. Jin, Y. Liu, X. Liu, K. Su, K. Shi, *Acta Pharm. Sin. B* **2021**, *11*, 2265.
[38] A. K. Pearce, R. K. O'Reilly, *Bioconjugate Chem.* **2019**, *30*, 2300.
[39] N. L. Anderson, N. G. Anderson, *Mol. Cell. Proteomics* **2002**, *1*, 845.
[40] M. Mahmoudi, N. Bertrand, H. Zope, O. C. Farokhzad, *Nano Today* **2016**, *11*, 817.
[41] D. Chen, S. Ganesh, W. Wang, M. Amiji, *Nanomedicine* **2017**, *12*, 2113.
[42] C. Corbo, R. Molinaro, A. Parodi, N. E. Toledano Furman, F. Salvatore, E. Tasciotti, *Nanomedicine* **2016**, *11*, 81.
[43] H.-Y. Kim, J. O. Sofo, D. Velegol, M. W. Cole, A. A. Lucas, *Langmuir* **2007**, *23*, 1735.
[44] Y. Min, M. Akbulut, K. Kristiansen, Y. Golan, J. Israelachvili, *Nat. Mater.* **2008**, *7*, 527.
[45] P. Aggarwal, J. B. Hall, C. B. Mcleland, M. A. Dobrovolskaia, S. E. Mcneil, *Adv. Drug Delivery Rev.* **2009**, *61*, 428.
[46] M. P. Monopoli, C. Aberg, A. Salvati, K. A. Dawson, *Nat. Nanotechnol.* **2012**, *7*, 779.
[47] N. Hoshyar, S. Gray, H. Han, G. Bao, *Nanomedicine* **2016**, *11*, 673.
[48] C. F. Rodrigues, N. Fernandes, D. De Melo-Diogo, P. Ferreira, I.-D. J. Correia, A. F. Moreira, *Nanomedicine* **2021**, *16*, 2569.
[49] M. Janát-Amsbury, A. Ray, C. Peterson, H. Ghandehari, *Eur. J. Pharm. Biopharm.* **2011**, *77*, 417.
[50] R. Toy, P. M. Peiris, K. B. Ghaghada, E. Karathanasis, *Nanomedicine* **2014**, *9*, 121.
[51] K. C. L. Black, Y. Wang, H. P. Luehmann, X. Cai, W. Xing, B.o Pang, Y. Zhao, C. S. Cutler, L. V. Wang, Y. Liu, Y. Xia, *ACS Nano* **2014**, *8*, 4385.
[52] H. Zhang, Y. Liu, M. Chen, X. Luo, X. Li, *J. Controlled Release* **2016**, *244*, 52.
[53] C. Sanchez-Cano, M. Carril, *Int. J. Mol. Sci.* **2020**, *21*, 1007.
[54] R. Rai, S. Alwani, I. Badea, *Polymers* **2019**, *11*, 745.
[55] S. Lowe, N. M. O'brien-Simpson, L. A. Connal, *Polym. Chem.* **2015**, *6*, 198.
[56] D. Nagasawa, T. Azuma, H. Noguchi, K. Uosaki, M. Takai, *J. Phys. Chem. C* **2015**, *119*, 17193.
[57] S. Chen, L. Li, C. Zhao, J. Zheng, *Polymer* **2010**, *51*, 5283.
[58] T. Mcpherson, A. Kidane, I. Szleifer, K. Park, *Langmuir* **1998**, *14*, 176.

[59] D. Shi, D. Beasock, A. Fessler, J. Szebeni, J. Y. Ljubimova, K. A. Afonin, M. A. Dobrovolskaia, *Adv. Drug Delivery Rev.* **2021**, *180*, 114079.
[60] J. L. Perry, K. G. Reuter, M. P. Kai, K. P. Herlihy, S. W. Jones, J. C. Luft, M. Napier, J. E. Bear, J. M. Desimone, *Nano Lett.* **2012**, *12*, 5304.
[61] Q.i Yang, S. W. Jones, C. L. Parker, W. C. Zamboni, J. E. Bear, S. K. Lai, *Mol. Pharmaceutics* **2014**, *11*, 1250.
[62] J. S. Suk, Q. Xu, N. Kim, J. Hanes, L. M. Ensign, *Adv. Drug Delivery Rev.* **2016**, *99*, 28.
[63] Y. He, J. Hower, S. Chen, M. T. Bernards, Y. Chang, S. Jiang, *Langmuir* **2008**, *24*, 10358.
[64] Q. Yang, S. K. Lai, *Wiley Interdiscip. Rev.: Nanomed. Nanobiotechnol.* **2015**, *7*, 655.
[65] C. Fang, B. Shi, Y.-Y. Pei, M.-H. Hong, J. Wu, H.-Z. Chen, *Eur. J. Pharm. Sci.* **2006**, *27*, 27.
[66] Q. He, J. Zhang, J. Shi, Z. Zhu, L. Zhang, W. Bu, L. Guo, Y.u Chen, *Biomaterials* **2010**, *31*, 1085.
[67] M. Miteva, K. C. Kirkbride, K. V. Kilchrist, T. A. Werfel, H. Li, C. E. Nelson, M. K. Gupta, T. D. Giorgio, C. L. Duvall, *Biomaterials* **2015**, *38*, 97.
[68] Y.u Mima, Y. Hashimoto, T. Shimizu, H. Kiwada, T. Ishida, *Mol. Pharmaceutics* **2015**, *12*, 2429.
[69] N. D'avanzo, C. Celia, A. Barone, M. Carafa, L. Di Marzio, H. A. Santos, M. Fresta, *Adv. Ther.* **2020**, *3*, 1900170.
[70] P. Zhang, F. Sun, S. Liu, S. Jiang, *J. Controlled Release* **2016**, *244*, 184.
[71] M. G. P. Saifer, L. D. Williams, M. A. Sobczyk, S. J. Michaels, M. R. Sherman, *Mol. Immunol.* **2014**, *57*, 236.
[72] K. Shiraishi, M. Hamano, H. Ma, K. Kawano, Y. Maitani, T. Aoshi, K. J. Ishii, M. Yokoyama, *J. Controlled Release* **2013**, *165*, 183.
[73] F. Wang, X. Ye, Y. Wu, H. Wang, C. Sheng, D. Peng, W. Chen, *J. Pharm. Sci.* **2019**, *108*, 641.
[74] Q. Yang, T. M. Jacobs, J. D. Mccallen, D. T. Moore, J. T. Huckaby, J. N. Edelstein, S. K. Lai, *Anal. Chem.* **2016**, *88*, 11804.
[75] H. Xu, W. Zhang, Y. Li, F. F. Ye, P. P. Yin, X. Yu, M. N. Hu, Y. S. Fu, C. Wang, D. J. Shang, *Pharm. Res.* **2014**, *31*, 3038.
[76] K. Xu, L. Zhang, Y. Gu, H. Yang, B. Du, H. Liu, Y. Li, *Eur. Polym. J.* **2021**, *145*, 110232.
[77] R. M. England, J. I. Moss, K. J. Hill, K. Elvevold, B Smedsrød, M. B. Ashford, *Biomater. Sci.* **2019**, *7*, 3418.
[78] T. Verbrugghen, B. D. Monnery, M. Glassner, S. Stroobants, R. Hoogenboom, S. Staelens, *J. Controlled Release* **2016**, *235*, 63.
[79] L. Wen, S. Huang, W. Du, C. Zhu, H. Xu, *Drug Dev. Ind. Pharm.* **2020**, *46*, 283.
[80] D. Pizzi, A. M. Mahmoud, T. Klein, J. P. Morrow, J. Humphries, Z. H. Houston, N. L. Fletcher, C. A. Bell, K. J. Thurecht, K. Kempe, *Eur. Polym. J.* **2021**, *151*, 110447.
[81] P. H. Kierstead, H. Okochi, V. J. Venditto, T. C. Chuong, S. Kivimae, J. M. J. Fréchet, F. C. Szoka, *J. Controlled Release* **2015**, *213*, 1.
[82] J. Humphries, D. Pizzi, S. E. Sonderegger, N. L. Fletcher, Z. H. Houston, C. A. Bell, K. Kempe, K. J. Thurecht, *Biomacromolecules* **2020**, *21*, 3318.
[83] C. Li, X.i Zhao, Y. Wang, H. Yang, H. Li, H. Li, W. Tian, J. Yang, J. Cui, *Int. J. Pharm.* **2013**, *443*, 17.
[84] R. Saadati, S. Dadashzadeh, Z. Abbasian, H. Soleimanjahi, *Pharm. Res.* **2013**, *30*, 985.
[85] B. Li, F. Chu, Q. Lu, Y. Wang, L. A. Lane, *Acta Biomater.* **2021**, *121*, 527.
[86] S. Liang, Y. Liu, X. Jin, G. Liu, J. Wen, L. Zhang, J. Li, X. Yuan, I. S. Y. Chen, W. Chen, H. Wang, L. Shi, X. Zhu, Y. Lu, *Nano Res.* **2016**, *9*, 1022.
[87] L. Zhang, Y. Liu, G. Liu, D. Xu, S. Liang, X. Zhu, Y. Lu, H. Wang, *Nano Res.* **2016**, *9*, 2424.
[88] H. Sun, L. Yan, R. Zhang, J. F. Lovell, Y. Wu, C. Cheng, *Biomater. Sci.* **2021**, *9*, 5000.
[89] K. P. García, K. Zarschler, L. Barbaro, J.-A. Barreto, W. O'Malley, L. Spiccia, H. Stephan, B. Graham, *Small* **2014**, *10*, 2516.
[90] S. Jiang, Z. Cao, *Adv. Mater.* **2010**, *22*, 920.
[91] J. Wu, W. Lin, Z. Wang, S. Chen, Y. Chang, *Langmuir* **2012**, *28*, 7436.
[92] S. Zhai, Y. Ma, Y. Chen, D. Li, J. Cao, Y. Liu, M. Cai, X. Xie, Y. Chen, X. Luo, *Polym. Chem.* **2014**, *5*, 1285.
[93] Q. Jin, Y. Chen, Y. Wang, J. Ji, *Colloids Surf., B* **2014**, *124*, 80.
[94] Q. Shao, Y.i He, S. Jiang, *J. Phys. Chem. B* **2011**, *115*, 8358.
[95] H. Ou, T. Cheng, Y. Zhang, J. Liu, Y. Ding, J. Zhen, W. Shen, Y. Xu, W. Yang, P. Niu, J. Liu, Y. An, Y. Liu, L. Shi, *Acta Biomater.* **2018**, *65*, 339.
[96] R. Xie, P. Yang, S. Peng, Y. Cao, X. Yao, S. Guo, W. Yang, *J. Mater. Chem. B* **2020**, *8*, 6128.
[97] S. Wang, F. Zhang, G. Yu, Z. Wang, O. Jacobson, Y. Ma, R. Tian, H. Deng, W. Yang, Z.-Y. Chen, X. Chen, *Theranostics* **2020**, *10*, 6629.
[98] L. Zhang, H. Xue, C. Gao, L. Carr, J. Wang, B. Chu, S. Jiang, *Biomaterials* **2010**, *31*, 6582.
[99] H. Idrees, S. Z. J. Zaidi, A. Sabir, R. U. Khan, X. Zhang, S.-U. Hassan, *Nanomaterials* **2020**, *10*, 1970.
[100] G. Huang, H. Huang, *J. Controlled Release* **2018**, *278*, 122.
[101] F. Abedini, M. Ebrahimi, A. H. Roozbehani, A. J. Domb, H. Hosseinkhani, *Polym. Adv. Technol.* **2018**, *29*, 2564.
[102] F. Oroojalian, M. Beygi, B. Baradaran, A. Mokhtarzadeh, M. A. Shahbazi, *Small* **2021**, *17*, 2006484.
[103] F. Castro, C. Martins, M. J. Silveira, R. P. Moura, C. L. Pereira, B. Sarmento, *Adv. Drug Delivery Rev.* **2021**, *170*, 312.
[104] L. Rao, L.-L. Bu, Q.-F. Meng, B. Cai, W.-W. Deng, A. Li, K. Li, S.-S. Guo, W.-F. Zhang, W. Liu, Z.-J. Sun, X.-Z. Zhao, *Adv. Funct. Mater.* **2017**, *27*, 1604774.
[105] H. Sun, J. Su, Q. Meng, Q. Yin, L. Chen, W. Gu, P. Zhang, Z. Zhang, H. Yu, S. Wang, Y. Li, *Adv. Mater.* **2016**, *28*, 9581.
[106] H.-Y. Chen, J. Deng, Y. Wang, C.-Q. Wu, X. Li, H.-W. Dai, *Acta Biomater.* **2020**, *112*, 1.
[107] L. Jing, H. Qu, D. Wu, C. Zhu, Y. Yang, X. Jin, J. Zheng, X. Shi, X. Yan, Y. Wang, *Theranostics* **2018**, *8*, 2683.
[108] L. Rao, L.-L. Bu, J.-H. Xu, B. Cai, G.-T. Yu, X. Yu, Z. He, Q. Huang, A. Li, S.-S. Guo, W.-F. Zhang, W. Liu, Z.-J. Sun, H. Wang, T.-H. Wang, X.-Z. Zhao, *Small* **2015**, *11*, 6225.
[109] Q. Xu, J. Wan, N. Bie, X. Song, X. Yang, T. Yong, Y. Zhao, X. Yang, L. Gan, *Theranostics* **2018**, *8*, 5362.
[110] A. Parodi, N. Quattrocchi, A. L. Van De Ven, C. Chiappini, M. Evangelopoulos, J. O. Martinez, B. S. Brown, S. Z. Khaled, I. K. Yazdi, M. V. Enzo, L. Isenhart, M. Ferrari, E. Tasciotti, *Nat. Nanotechnol.* **2013**, *8*, 61.
[111] C. Gao, Z. Lin, B. Jurado-Sánchez, X. Lin, Z. Wu, Q. He, *Small* **2016**, *12*, 4056.
[112] Q.-F. Meng, L. Rao, M. Zan, M. Chen, G.-T. Yu, X. Wei, Z. Wu, Y. Sun, S.-S. Guo, X.-Z. Zhao, F.-B. Wang, W. Liu, *Nanotechnology* **2018**, *29*, 134004.
[113] Z. Chen, P. Zhao, Z. Luo, M. Zheng, H. Tian, P. Gong, G. Gao, H. Pan, L. Liu, A. Ma, H. Cui, Y. Ma, L. Cai, *ACS Nano* **2016**, *10*, 10049.
[114] P. Guo, J. Huang, Y. Zhao, C. R. Martin, R. N. Zare, M. A. Moses, *Small* **2018**, *14*, 1703493.
[115] L. Rao, B. Cai, L.-L. Bu, Q.-Q. Liao, S.-S. Guo, X.-Z. Zhao, W.-F. Dong, W. Liu, *ACS Nano* **2017**, *11*, 3496.
[116] D. Shao, F. Zhang, F. Chen, X. Zheng, H. Hu, C. Yang, Z. Tu, Z. Wang, Z. Chang, J. Lu, T. Li, Y. Zhang, L.i Chen, K. W. Leong, W. F. Dong, *Adv. Mater.* **2020**, *32*, 2004385.
[117] D. Shao, M. Li, Z. Wang, X. Zheng, Y.-H. Lao, Z. Chang, F. Zhang, M. Lu, J. Yue, H. Hu, H. Yan, L.i Chen, W.-F. Dong, K. W. Leong, *Adv. Mater.* **2018**, *30*, 1801198.
[118] Y. Li, T. Yan, W. Chang, C. Cao, D. Deng, *Biomater. Sci.* **2019**, *7*, 3652.
[119] J. Su, H. Sun, Q. Meng, Q. Yin, S. Tang, P. Zhang, Y. Chen, Z. Zhang, H. Yu, Y. Li, *Adv. Funct. Mater.* **2016**, *26*, 1243.

[120] S. Ong, M. Chitneni, K. Lee, L. Ming, K. Yuen, *Pharmaceutics* **2016**, *8*, 36.
[121] B. T. Luk, Y. Jiang, J. A. Copp, C.-M. J. Hu, N. Krishnan, W. Gao, S. Li, R. H. Fang, L. Zhang, *Mol. Pharmaceutics* **2018**, *15*, 3723.
[122] T. Kang, Q. Zhu, D. Wei, J. Feng, J. Yao, T. Jiang, Q. Song, X. Wei, H. Chen, X. Gao, J. Chen, *ACS Nano* **2017**, *11*, 1397.
[123] D. Dehaini, X. Wei, R. H. Fang, S. Masson, P. Angsantikul, B. T. Luk, Y. Zhang, M. Ying, Y. Jiang, A. V. Kroll, W. Gao, L. Zhang, *Adv. Mater.* **2017**, *29*, 1606209.
[124] F. Yang, M. H. Cabe, S. D. Ogle, V. Sanchez, K. A. Langert, *Sci. Rep.* **2021**, *11*, 23996.
[125] Z. A. Nizamudeen, R. Xerri, C. Parmenter, K. Suain, R. Markus, L. Chakrabarti, V. Sottile, *Cells* **2021**, *10*, 2413.
[126] Z. Wang, F. Zhang, D. Shao, Z. Chang, L. Wang, H. Hu, X. Zheng, X. Li, F. Chen, Z. Tu, M. Li, W. Sun, L.i Chen, W. F. Dong, *Adv. Sci.* **2019**, *6*, 1901690.
[127] H. Ren, J. Liu, Y. Li, H. Wang, S. Ge, A. Yuan, Y. Hu, J. Wu, *Acta Biomater.* **2017**, *59*, 269.
[128] L. Zhang, Q. Chen, Y. Ma, J. Sun, *ACS Appl. Bio Mater.* **2019**, *3*, 107.
[129] S. Ye, F. Wang, Z. Fan, Q. Zhu, H. Tian, Y. Zhang, B. Jiang, Z. Hou, Y. Li, G. Su, *ACS Appl. Mater. Interfaces* **2019**, *11*, 15262.
[130] S. A. Alqahtani, G. I. Harisa, A. H. Alomrani, F. K. Alanazi, M. M. Badran, *Colloids Surf., B* **2021**, *197*, 111380.
[131] X. Wang, H. Li, X. Liu, Y. Tian, H. Guo, T. Jiang, Z. Luo, K. Jin, X. Kuai, Y. Liu, Z. Pang, W. Yang, S. Shen, *Biomaterials* **2017**, *143*, 130.
[132] M. Gao, C. Liang, X. Song, Q. Chen, Q. Jin, C. Wang, Z. Liu, *Adv. Mater.* **2017**, *29*, 1701429.
[133] B. Liu, W. Wang, J. Fan, Y. Long, F. Xiao, M. Daniyal, C. Tong, Q. Xie, Y. Jian, B. Li, X. Ma, W. Wang, *Biomaterials* **2019**, *217*, 119301.
[134] W. Liu, M. Ruan, Y. Wang, R. Song, X. Ji, J. Xu, J. Dai, W. Xue, *Small* **2018**, *14*, 1801754.
[135] J. Fan, B. Liu, Y. Long, Z. Wang, C. Tong, W. Wang, P. You, X. Liu, *Acta Biomater.* **2020**, *113*, 554.
[136] Q. Hu, W. Sun, C. Qian, C. Wang, H. N. Bomba, Z. Gu, *Adv. Mater.* **2015**, *27*, 7043.
[137] H. Zuo, J. Tao, H. Shi, J. He, Z. Zhou, C. Zhang, *Acta Biomater.* **2018**, *80*, 296.
[138] C. Chi, F. Li, H. Liu, S. Feng, Y. Zhang, D.a Zhou, R. Zhang, *J. Nanopart. Res.* **2019**, *21*, 144.
[139] P. Kumar, T. V. Treuren, A. P. Ranjan, P. Chaudhary, J. K. Vishwanatha, *Nanotechnology* **2019**, *30*, 265101.
[140] W. Zhang, M. Yu, Z. Xi, D. Nie, Z. Dai, J. Wang, K. Qian, H. Weng, Y. Gan, L. Xu, *ACS Appl. Mater. Interfaces* **2019**, *11*, 46614.
[141] X. Zheng, Y. Zhao, Y. Jia, D. Shao, F. Zhang, M. Sun, J. Dawulieti, H. Hu, L. Cui, Y. Pan, C. Yang, W. Sun, S. Zhang, K. He, J. Li, J. Du, M. Zhang, L.i Chen, *Biomaterials* **2021**, *271*, 120716.
[142] X. Ren, S. Yang, N. Yu, A. Sharjeel, Q. Jiang, D. K. Macharia, H. Yan, C. Lu, P. Geng, Z. Chen, *J. Colloid Interface Sci.* **2021**, *591*, 229.
[143] M. Xuan, J. Shao, L. Dai, J. Li, Q. He, *ACS Appl. Mater. Interfaces* **2016**, *8*, 9610.
[144] X. Cao, T. Tan, D. Zhu, H. Yu, Y. Liu, H. Zhou, Y. Jin, Q. Xia, *Int. J. Nanomed.* **2020**, *15*, 1915.
[145] X. Zhou, R. Yu, X. Cao, Z.-R. Zhang, L. Deng, *J. Biomed. Nanotechnol.* **2019**, *15*, 993.
[146] G. Deng, Z. Sun, S. Li, X. Peng, W. Li, L. Zhou, Y. Ma, P. Gong, L. Cai, *ACS Nano* **2018**, *12*, 12096.
[147] Y. Han, H. Pan, W. Li, Z. Chen, A. Ma, T. Yin, R. Liang, F. Chen, Y. Ma, Y. Jin, M. Zheng, B. Li, L. Cai, *Adv. Sci.* **2019**, *6*, 1900251.
[148] Q. Jiang, Y. Liu, R. Guo, X. Yao, S. Sung, Z. Pang, W. Yang, *Biomaterials* **2019**, *192*, 292.
[149] D. Wang, H. Dong, M. Li, Y. Cao, F. Yang, K. Zhang, W. Dai, C. Wang, X. Zhang, *ACS Nano* **2018**, *12*, 5241.
[150] Q. Peng, H. Li, Q. Deng, L. Liang, F. Wang, Y. Lin, L. Yang, Y. Zhang, X. Yu, L. Zhang, *J. Colloid Interface Sci.* **2021**, *603*, 319.
[151] C. Gong, X. Yu, B. You, Y. Wu, R. Wang, L. Han, Y. Wang, S. Gao, Y. Yuan, *J. Nanobiotechnol.* **2020**, *18*, 92.
[152] H. He, C. Guo, J. Wang, W. J. Korzun, X.-Y. Wang, S. Ghosh, H. Yang, *Nano Lett.* **2018**, *18*, 6164.
[153] H. Li, Q. Peng, L. Yang, Y. Lin, S. Chen, Y. Qin, S. Li, X. Yu, L. Zhang, *ACS Appl. Mater. Interfaces* **2020**, *12*, 57732.
[154] W. L. Liu, M. Z. Zou, T. Liu, J. Y. Zeng, X. Li, W. Y. Yu, C. X. Li, J. J. Ye, W. Song, J. Feng, X. Z. Zhang, *Adv. Mater.* **2019**, *31*, 1900499.
[155] J. Xiong, M. Wu, J. Chen, Y. Liu, Y. Chen, G. Fan, Y. Liu, J. Cheng, Z. Wang, S. Wang, Y.i Liu, W. Zhang, *ACS Nano* **2021**, *15*, 19756.
[156] Y. Liu, X. Wang, B. Ouyang, X. Liu, Y. Du, X. Cai, H. Guo, Z. Pang, W. Yang, S. Shen, *J. Mater. Chem. B* **2018**, *6*, 7033.
[157] M. Sun, Y. Duan, Y. Ma, Q. Zhang, *Int. J. Nanomed.* **2020**, *15*, 6749.
[158] V. R. Muzykantov, *Expert Opin. Drug Delivery* **2010**, *7*, 403.
[159] M. Moras, S. D. Lefevre, M. A. Ostuni, *Front. Physiol.* **2017**, *8*, 1076.
[160] P. Burger, P. Hilarius-Stokman, D. De Korte, T. K. Van Den Berg, R. Van Bruggen, *Blood* **2012**, *119*, 5512.
[161] R. H. Fang, C.-M. J. Hu, L. Zhang, in *Nanoparticles Disguised as Red Blood Cells to Evade the Immune System*, Taylor & Francis, London **2012**, p. 385.
[162] Q. Xia, Y. Zhang, Z. Li, X. Hou, N. Feng, *Acta Pharm. Sin. B* **2019**, *9*, 675.
[163] C.-M. J. Hu, L.i Zhang, S. Aryal, C. Cheung, R. H. Fang, L. Zhang, *Proc. Natl. Acad. Sci. USA* **2011**, *108*, 10980.
[164] J. N. Thon, J. E. Italiano, *Antiplatelet Agents* **2012**, *210*, 3.
[165] K. R. Machlus, J. N. Thon, J. E. Italiano, *Br. J. Haematol.* **2014**, *165*, 227.
[166] M. R. Yeaman, *Cell. Mol. Life Sci.* **2010**, *67*, 525.
[167] C. L. Modery-Pawlowski, L. L. Tian, V. Pan, K. R. Mccrae, S. Mitragotri, A. Sen Gupta, *Biomaterials* **2013**, *34*, 526.
[168] Z. Li, S. Hu, K. Cheng, *J. Mater. Chem. B* **2018**, *6*, 7354.
[169] S. S. Kunde, S. Wairkar, *Int. J. Pharm.* **2021**, *598*, 120395.
[170] Y. Song, Z. Huang, X. Liu, Z. Pang, J. Chen, H. Yang, N. Zhang, Z. Cao, M. Liu, J. Cao, C. Li, X. Yang, H. Gong, J. Qian, J. Ge, *Nanomed.-Nanotechnol. Biol. Med.* **2019**, *15*, 13.
[171] M. Olsson, P. Bruhns, W. A. Frazier, J. V. Ravetch, P.-A. Oldenborg, *Blood* **2005**, *105*, 3577.
[172] C.-M. J. Hu, R. H. Fang, K.-C. Wang, B. T. Luk, S. Thamphiwatana, D. Dehaini, P. Nguyen, P. Angsantikul, C. H. Wen, A. V. Kroll, C. Carpenter, M. Ramesh, V. Qu, S. H. Patel, J. Zhu, W. Shi, F. M. Hofman, T. C. Chen, W. Gao, K. Zhang, S. Chien, L. Zhang, *Nature* **2015**, *526*, 118.
[173] J. Li, Y. Ai, L. Wang, P. Bu, C. C. Sharkey, Q. Wu, B. Wun, S. Roy, X. Shen, M. R. King, *Biomaterials* **2016**, *76*, 52.
[174] L. A. Plantureux, L. Crescence, F. Dignat-George, L. Panicot-Dubois, C. Dubois, *Thromb. Res.* **2018**, *164*, S40.
[175] M. Labelle, S. Begum, R. O. Hynes, *Proc. Natl. Acad. Sci. USA* **2014**, *111*, E3053.
[176] T. M. Getz, R. K. Montgomery, J. A. Bynum, J. K. Aden, H. F. Pidcoke, A. P. Cap, *Transfusion* **2016**, *56*, 1320.
[177] J. Jin, Z. M. Bhujwalla, *Front. Oncol.* **2020**, *9*, 1560.
[178] F. Jin, J. Qi, D.i Liu, Y. You, G. Shu, Y. Du, J. Wang, X. Xu, X. Ying, J. Ji, Y. Du, *J. Controlled Release* **2021**, *337*, 90.
[179] J. Jin, B. Krishnamachary, J. D. Barnett, S. Chatterjee, D. Chang, Y. Mironchik, F. Wildes, E. M. Jaffee, S. Nimmagadda, Z. M. Bhujwalla, *ACS Appl. Mater. Interfaces* **2019**, *11*, 7850.
[180] Q. Sun, J. Wu, L. Jin, L. Hong, F. Wang, Z. Mao, M. Wu, *J. Mater. Chem. B* **2020**, *8*, 7253.
[181] D. Nie, Z. Dai, J. Li, Y. Yang, Z. Xi, J. Wang, W. Zhang, K. Qian, S. Guo, C. Zhu, R. Wang, Y. Li, M. Yu, X. Zhang, X. Shi, Y. Gan, *Nano Lett.* **2019**, *20*, 936.
[182] R. Yang, J. Xu, L. Xu, X. Sun, Q. Chen, Y. Zhao, R. Peng, Z. Liu, *ACS Nano* **2018**, *12*, 5121.

[183] S. Banskota, P. Yousefpour, A. Chilkoti, *Macromol. Biosci.* **2017**, *17*, 1600361.
[184] S. Shalapour, M. Karin, *J. Clin. Invest.* **2015**, *125*, 3347.
[185] K. J. Hiam-Galvez, B. M. Allen, M. H. Spitzer, *Nat. Rev. Cancer* **2021**, *21*, 345.
[186] D. Hanahan, *Cancer Discovery* **2022**, *12*, 31.
[187] R. Noy, J. W. Pollard, *Immunity* **2014**, *41*, 49.
[188] Q. Chen, X. H.-F. Zhang, J. Massagué, *Cancer Cell* **2011**, *20*, 538.
[189] Q. He, S. Guo, Z. Qian, X. Chen, *Chem. Soc. Rev.* **2015**, *44*, 6258.
[190] S. M. Pyonteck, L. Akkari, A. J. Schuhmacher, R. L. Bowman, L. Sevenich, D. F. Quail, O. C. Olson, M. L. Quick, J. T. Huse, V. Teijeiro, M. Setty, C. S. Leslie, Y. Oei, A. Pedraza, J. Zhang, C. W. Brennan, J. C. Sutton, E. C. Holland, D. Daniel, J. A. Joyce, *Nat. Med.* **2013**, *19*, 1264.
[191] A. Mantovani, F. Marchesi, A. Malesci, L. Laghi, P. Allavena, *Nat. Rev. Clin. Oncol.* **2017**, *14*, 399.
[192] C. Chen, M. Song, Y. Du, Y. Yu, C. Li, Y. Han, F. Yan, Z. Shi, S. Feng, *Nano Lett.* **2021**, *21*, 5522.
[193] H. Wang, J. Zang, Z. Zhao, Q. Zhang, S. Chen, *Int. J. Nanomed.* **2021**, *16*, 7663.
[194] S. Xiong, L. Dong, L. Cheng, *J. Hematol. Oncol.* **2021**, *14*, 173.
[195] L. Tang, S. He, Y. Yin, J. Li, Q. Xiao, R. Wang, L. Gao, W. Wang, *Nanoscale* **2022**, *14*, 1621.
[196] X. Cao, Y. Hu, S. Luo, Y. Wang, T. Gong, X. Sun, Y. Fu, Z. Zhang, *Acta Pharm. Sin. B* **2019**, *9*, 575.
[197] T. Bald, M. F. Krummel, M. J. Smyth, K. C. Barry, *Nat. Immunol.* **2020**, *21*, 835.
[198] C. Guillerey, N. D. Huntington, M. J. Smyth, *Nat. Immunol.* **2016**, *17*, 1025.
[199] L. Wu, F. Zhang, Z. Wei, X. Li, H. Zhao, H. Lv, R. Ge, H.e Ma, H. Zhang, B. Yang, J. Li, J. Jiang, *Biomater. Sci.* **2018**, *6*, 2714.
[200] A. Pitchaimani, T. D. T. Nguyen, S. Aryal, *Biomaterials* **2018**, *160*, 124.
[201] H. Klingemann, L. Boissel, F. Toneguzzo, *Front. Immunol.* **2016**, *7*, 91.
[202] J. Zhang, H. Zheng, Y. Diao, *Int. J. Mol. Sci.* **2019**, *20*, 317.
[203] A. Gardner, B. Ruffell, *Trends Immunol.* **2016**, *37*, 855.
[204] K. F. Bol, G. Schreibelt, W. R. Gerritsen, I. J. M. De Vries, C. G. Figdor, *Clin. Cancer Res.* **2016**, *22*, 1897.
[205] A. D. Garg, L. Vandenberk, C. Koks, T. Verschuere, L. Boon, S. W. Van Gool, P. Agostinis, *Sci. Transl. Med.* **2016**, *8*, 328ra27.
[206] S. I. M. Sutherland, X. Ju, L. G. Horvath, G. J. Clark, *Front. Immunol.* **2021**, *12*, 562.
[207] L. J. Ochyl, J. J. Moon, *Adv. Healthcare Mater.* **2019**, *8*, 1801091.
[208] S. Cheng, C. Xu, Y. Jin, Y. Li, C. Zhong, J. Ma, J. Yang, N. Zhang, Y. Li, C. Wang, Z. Yang, Y.u Wang, *Adv. Sci.* **2020**, *7*, 1903301.
[209] W. Ma, D. Zhu, J. Li, X. Chen, W. Xie, X. Jiang, L. Wu, G. Wang, Y. Xiao, Z. Liu, F. Wang, A. Li, D. Shao, W. Dong, W. Liu, Y. Yuan, *Theranostics* **2020**, *10*, 1281.
[210] Z. Zeng, K. Pu, *Adv. Funct. Mater.* **2020**, *30*, 2004397.
[211] H. Raskov, A. Orhan, J. P. Christensen, I. Gögenur, *Br. J. Cancer* **2021**, *124*, 359.
[212] D. M. Mosser, J. P. Edwards, *Nat. Rev. Immunol.* **2008**, *8*, 958.
[213] L. Rao, Q.-F. Meng, Q. Huang, Z. Wang, G.-T. Yu, A. Li, W. Ma, N. Zhang, S.-S. Guo, X.-Z. Zhao, K. Liu, Y. Yuan, W. Liu, *Adv. Funct. Mater.* **2018**, *28*, 1803531.
[214] D. Wang, C. Liu, S. You, K. Zhang, M. Li, Y. Cao, C. Wang, H. Dong, X. Zhang, *ACS Appl. Mater. Interfaces* **2020**, *12*, 41138.
[215] Y. Liu, U. K. Sukumar, M. Kanada, A. Krishnan, T. F. Massoud, R. Paulmurugan, *Adv. Funct. Mater.* **2021**, *31*, 2103600.
[216] A. Villa, M. Garofalo, D. Crescenti, N. Rizzi, E. Brunialti, A. Vingiani, P. Belotti, C. Sposito, S. Franzè, F. Cilurzo, G. Pruneri, C. Recordati, C. Giudice, A. Giordano, M. Tortoreto, G. Beretta, D. Stefanello, G. Manenti, N. Zaffaroni, V. Mazzaferro, P. Ciana, *Theranostics* **2021**, *11*, 2034.
[217] V. Gambardella, N. Tarazona, J. M. Cejalvo, P. Lombardi, M. Huerta, S. Roselló, T. Fleitas, D. Roda, A. Cervantes, *Cancers* **2020**, *12*, 1009.
[218] N. Lafuente-GóMez, A. Latorre, P. Milán-Rois, C. Rodriguez Diaz, Á. L. Somoza, *Chem. Commun.* **2021**, *57*, 13662.
[219] C. F. Rodrigues, T. A. Jacinto, A. F. Moreira, E. C. Costa, S. P. Miguel, I.-D. J. Correia, *Nano Res.* **2019**, *12*, 719.

Carolina F. Rodrigues received her B.Sc. and M.Sc. degrees in biomedical sciences from the University of Beira Interior in 2016 and 2018, respectively. She is now a Ph.D. student in biomedicine at the same university. Her research interests are focused on the development and functionalization of gold-based nanomaterials for application in cancer photothermal therapy and biomedicine.

Ilídio J. Correia is a full professor in the Department of Health Sciences at the University of Beira Interior. He obtained his B.Sc. and Ph.D. degrees in biochemistry from the University of Lisbon in 1998 and New University of Lisbon in 2003, respectively. His research group is involved in the development of skin and bone substitutes, drug delivery systems, as well as in vitro 3D cell culture models of cancer.

André F. Moreira is an invited adjunct professor at the Instituto Politécnico da Guarda (IPG) and an invited assistant professor at the University of Beira Interior (UBI). In 2019, he completed his Ph.D. degree in biochemistry at UBI. Since then, he has continued to develop his research at the CICS-UBI research center and UDI-IPG. His research interests are focused on the application of macroscale drug delivery systems (e.g., microneedles) and gold core–silica shell nanoparticles in cancer therapy, developing multifunctional agents capable of combining the therapeutic, i.e., drug delivery and photothermal therapy, and imaging functionalities.